Identifying Meteorological Controls on Open and Closed Mesoscale Cellular Convection Associated with Marine Cold Air Outbreaks

Isabel L. McCoy[1], Robert Wood[1], Jennifer K. Fletcher[2]

[1]Atmospheric Sciences, University of Washington, Seattle, Washington, USA

[2]School of Earth and Environment, University of Leeds, Leeds, UK

Corresponding author: I. L. McCoy (imccoy@uw.edu)

Key Points:

- A near global satellite dataset of marine low cloud is used to determine meteorological drivers of mesoscale cellular convection (MCC).
- A marine cold air outbreak index combining both surface forcing and lower tropospheric stability is shown to be a good predictor of MCC.
- MCC types have different albedo-cloud fraction relationships indicating that mesoscale morphology is important for radiative impacts.

Abstract

Mesoscale cellular convective (MCC) clouds occur in large-scale patterns over the ocean and have important radiative effects on the climate system. An examination of time-varying meteorological conditions associated with satellite-observed open and closed MCC is conducted to illustrate the influence of large-scale meteorological conditions on cloud development. Marine cold air outbreaks (MCAO) influence the development of open MCC and the transition from closed to open MCC. MCC neural network classifications on MODIS data for 2008 are collocated with CERES data and ERA-Interim Reanalysis to determine the radiative effects of MCC and their thermodynamic environments. Closed MCC are found to have much higher albedo on average than open MCC for the same cloud fraction. Three metrics for meteorological controls are tested for MCC predictive ability: sea-air temperature difference (ΔT), estimated inversion strength (EIS), and a MCAO index (M). These metrics illustrate the importance of atmospheric surface forcing and static stability for open and closed MCC formation. Predictive sigmoidal relations are found between M and MCC frequency: strong and positive for open MCC, weaker and negative for closed MCC. The seasonal cycle of open MCC is most correlated with M, while the seasonality of closed MCC is most correlated with EIS. Open and closed MCC are, on average, best distinguished by M of all the metrics tested. The possibility of a MCC cloud feedback is discussed.

1 Introduction

Marine boundary layer clouds are key influencers of the climate system. They have important radiative impacts through strongly enhancing shortwave reflection and trapping longwave radiation [*D. L. Hartmann and Short*, 1980]. These radiative effects, as well as latent heat

production through precipitation, play a key role in the global energy budget [*Wood*, 2012]. Boundary layer clouds critically impact surface and top of atmosphere (TOA) energy budgets through their influence on the solar radiation budget in the high and mid-latitudes, especially the Artic and Southern Ocean (SO) [*Bennartz et al.*, 2013; *Bodas-Salcedo et al.*, 2016]. The complex microphysics and dynamic processes of low clouds have garnered much interest in recent years because low clouds are a leading contribution to the uncertainty in the changing energy budget in climate models [*Boucher*, 2013]. The model uncertainty from cloud feedbacks and cloud-aerosol interactions is due in part to difficulties in parameterizing the sub-grid scale processes important for these clouds [*Boucher*, 2013]. Bias in modeling of surface and TOA radiative fluxes in the Southern Ocean (SO) is an excellent example of this problem and motivational for this work. Correct representation of the radiative fluxes in the SO is important for accurately predicting global warming effects in a coupled atmosphere-ocean model [*Trenberth and Fasullo*, 2010; *Bodas-Salcedo et al.*, 2016]. Problems in cloud amount and brightness in the SO result in radiation biases that lead to inaccurate energy budgets and atmosphere and ocean transport [*Trenberth and Fasullo*, 2010]. SO biases are found to be associated with poor simulation of low and mid-level clouds, particularly those occurring in the cold sector of cyclones and in marine cold air outbreaks [*Field et al.*, 2011; *Bodas-Salcedo et al.*, 2012; *Williams et al.*, 2013; *Naud et al.*, 2014; *Bodas-Salcedo et al.*, 2016; *Kay et al.*, 2016]. Marine cold air outbreaks (MCAO) are movements of cold air from the poles equatorward over comparatively warmer water [*J Fletcher et al.*, 2016a; *Abel et al.*, 2017 (in press)]. MCAO are known to influence development of low clouds as the warm water-cool air contrast increases the flux of energy and moisture from the surface into the boundary layer [*Brummer*, 1996; *Kolstad et al.*, 2009; *J K Fletcher et al.*, 2016b; *Abel et al.*, 2017 (in press)]. *Papritz et al.* [2015] found that the seasonality and strength of the

Southern Ocean turbulent heat flux (latent plus sensible heat flux) is strongly controlled by cold air outbreaks. Models are especially poor at simulating the super cooled liquid clouds that dominate the low cloud population in the high latitudes, significant contributors to reflected shortwave between 70° and 40°S [*Forbes and Ahlgrimm*, 2014; *Bodas-Salcedo et al.*, 2016]. Super cooled clouds are controlled by complex, sub-grid scale mixed-phase processes (e.g. nucleation, secondary ice formation, Bergeron-Findeisen) that are known to be poorly parametrized in models [*Morrison et al.*, 2012; *Field et al.*, 2014; *McCoy et al.*, 2016]. Some reduction in SO biases has been achieved by implementing improved microphysics and boundary layer schemes in certain models [*Bodas-Salcedo et al.*, 2012; *Field et al.*, 2014]. This suggests that to find a complete solution to the SO and, more broadly, the mid-latitude biases exhibited in models, a profound understanding of the processes associated with the clouds occurring in these regions must be developed. This understanding, especially of clouds in cyclone cold sectors and MCAO, could be used to further improve and implement parameterizations in models. As these clouds are in the "grey zone", where some model resolutions are growing close to the convective scale of the cells but may not resolve all the mesoscale circulations, parameterizations that comprehensively capture the multiple scales are important but difficult to achieve [*Tomassini et al.*, 2016].

What clouds occur near and within these difficult-to-model, dynamic systems? To answer that, we first classify marine boundary layer

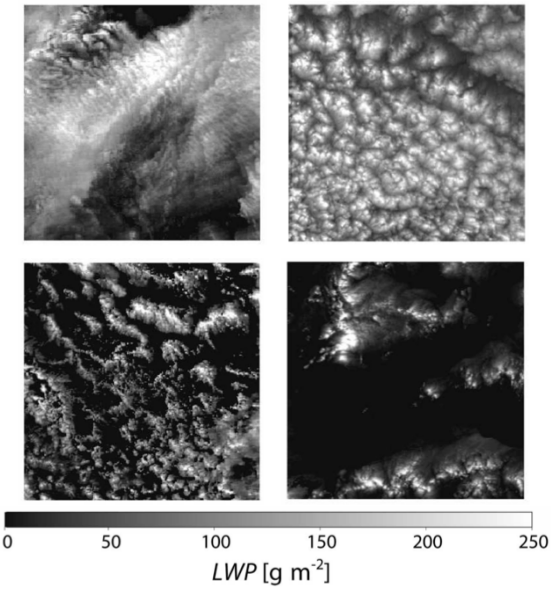

Figure 1 Example LWP of sub-scenes classified by the neural network algorithm into the four types (clockwise from top left): no MCC, closed MCC, cellular but disorganized, and open MCC.

clouds broadly based on their cellular morphology (Figure 1): open mesoscale cellular convection (MCC), closed MCC, no MCC, and cellular but disorganized MCC [*Wood and Hartmann*, 2006]. Open and closed MCC are organized into cellular patterns on the order of 10-40 km; cellular but disorganized has cellular clouds but lacks the large-scale organization of cells observed in open and closed MCC; and no MCC lacks both the cellularity and large-scale structure [*Atkinson and Zhang*, 1996; *Wood and Hartmann*, 2006]. Open MCC can be thought of as cumulus clouds arranged in hexagonal rings with a clear, descending region in the center. Closed MCC are essentially hexagonally shaped cells of stratocumulus clouds arranged into a large-scale pattern with clear, descending cell edges [*Atkinson and Zhang*, 1996]. Cellular but disorganized is the most prominent cloud type in this grouping, occurring over tropical regions in high quantities throughout the year. Crucially, open and closed MCC dominate the mid-latitudes and sub-tropical stratocumulus decks (e.g. Peruvian, Namibian, etc.) [*Klein and Hartmann*, 1993; *Muhlbauer et al.*, 2014]. These morphology types can loosely be thought of as different stages of the stratus to cumulus transitions observed over the eastern tropical and sub-tropical oceans [*Wood*, 2012]. In the high and mid-latitudes, a parallel transition is observed to occur between closed MCC (stratocumulus-like) to open MCC (cumulus-like). This transition is associated with the passage of cyclones and cold air outbreaks [*Atkinson and Zhang*, 1996; *Field et al.*, 2014; *J K Fletcher et al.*, 2016b; *Abel et al.*, 2017 (in press)]. Closed and open MCC dominate the mid-latitudes and are potentially the difficult to model clouds associated with cyclones and cold air outbreaks [*Muhlbauer et al.*, 2014; *J K Fletcher et al.*, 2016b]. Additionally, recent observations have confirmed that the stratocumulus/closed MCC to open MCC transition in cold air outbreaks often involves mixed-phase and super cooled clouds,

adding complexity to parameterizing these clouds for the previously stated reasons [*Abel et al.*, 2017 (in press)].

To improve understanding of how these clouds behave, one must understand the important drivers of open and closed MCC. Mesoscale cellular convective clouds were first observed in the early 1960's with the dawn of the satellite era [*Agee et al.*, 1973; *Agee*, 1984; 1987; *Atkinson and Zhang*, 1996]. Open and closed MCC have sufficiently large structures, with cell sizes often larger than 10km, that satellites were needed to observe their distinctive patterns. Such cellular convection had only been observed in the laboratory prior to these satellite sightings [*Bénard*, 1901; *Rayleigh*, 1916; *Atkinson and Zhang*, 1996]. Laboratory convective cells were created by heating thin layers of fluid from below, producing thermal instability in the fluid, and letting surface tension [*Bénard*, 1901] and buoyancy [*Rayleigh*, 1916] effects create convection. Given this set up, it is not surprising that open and closed MCC are an atmospheric parallel to the buoyancy driven cellular convection, known as Bénard-Rayleigh cells, although real-world effects like latent heating create formation differences [*Atkinson and Zhang*, 1996]. The complexities of these influences is aptly summarized by *Agee* [1987] at the end of his detailed comparison between laboratory and atmospheric cells:

> *Similarities and differences have been duly noted, but atmospheric convection is subjected to a myriad of physical processes that are external to the thermally-driven convective overturning… Atmospheric convectionists should never fall into the trap of categorically stating that a particular convective structure is always caused by a single external forcing mechanism. Over and over this is seen not to be the case…*

The important influences on MCC development have become clearer since the 1960's and 70's, particularly after the advent of large eddy simulations (LES) and in-situ observations. Many of

132 the processes key in stratocumulus clouds are important for MCC: shortwave heating and
133 longwave cooling at cloud top; turbulence and entrainment; drizzle, latent heating and
134 evaporative cooling; and surface fluxes of energy and moisture [*Wood*, 2012]. Atmospheric static
135 stability is also important and can be controlled by numerous factors including the cloud itself
136 and synoptic meteorology. Open MCC are particularly influenced by surface forcing while
137 closed MCC are more affected by longwave cloud-top cooling outside the sub-tropics [*Wood*,
138 2012; *Kazil et al.*, 2014].

139 Two of the most investigated mechanisms for the transition and breakup of closed into open
140 MCC are cloud-aerosol-precipitation interactions and advection over warmer water [*Yamaguchi*
141 *and Feingold*, 2015]. These two mechanisms can be thought of as microphysically driven and
142 large-scale meteorologically driven, respectively. The former has been substantiated through
143 numerous LES modeling and observational studies [*Stevens et al.*, 2005; *Savic-Jovcic and*
144 *Stevens*, 2008; *Xue et al.*, 2008; *Feingold et al.*, 2010; *Berner et al.*, 2013]. Development of
145 precipitation in closed MCC clouds can initiate cold pools, which spread out at the surface and
146 interact. Collision of cold pools at the surface produces updrafts and an upward flux of energy
147 and moisture. Closed MCC begins to break up in locations of precipitation. In regions of
148 enhanced surface forcing, cloud is sustained and forms the convective cells of new open MCC
149 [*Savic-Jovcic and Stevens*, 2008; *Wood et al.*, 2011; *Berner et al.*, 2013]. Cold pools are not
150 necessary for the closed to open transition to occur, as a recent LES study showed that
151 precipitation applied evenly across the domain can also drive the transition [*Vogel et al.*, 2016].
152 This is consistent with precipitation being found a necessary but insufficient condition for this
153 transition to occur [*Wood*, 2012; *Yamaguchi and Feingold*, 2015]. Closed to open transitions
154 may be influenced by aerosol suppression of precipitation in closed MCC [*Rosenfeld et al.*, 2006;

155 *Xue et al.*, 2008]. Meteorological conditions, specifically stronger subsidence, can also suppress
156 this transition by reducing the cloud thickness and preventing strong precipitation formation
157 [*Berner et al.*, 2013]. The second, meteorologically driven mechanism involves the advection of
158 cloud over warmer water [*Bretherton and Wyant*, 1997; *Wyant et al.*, 1997; *Sandu and Stevens*,
159 2011]. As the cloud moves over a comparatively warmer surface, an increase in the surface flux
160 of moisture occurs. This liberates more latent heating in clouds, driving stronger updrafts and
161 enhancing cloud top entrainment of warm, dry free tropospheric air which drives boundary layer
162 decoupling. Along with decoupling, liquid water path (LWP) is enhanced in geometrically
163 thicker clouds which may additionally lead to precipitation [*Bretherton and Wyant*, 1997; *Wyant*
164 *et al.*, 1997; *Sandu and Stevens*,
165 2011; *Wood*, 2012]. While these
166 studies are of the subtropical
167 stratocumulus to trade cumulus
168 transition, a parallel can be made to
169 the transition from closed to open
170 MCC [*Yamaguchi and Feingold*,
171 2015]. This mechanism could
172 explain the influence of large scale
173 meteorology in MCC transitions seen
174 in MCAO and cyclones [*Atkinson*
175 *and Zhang*, 1996; *Muller and*
176 *Chlond*, 1996; *Wood*, 2012; *J*
177 *Fletcher et al.*, 2016a]. Transitions

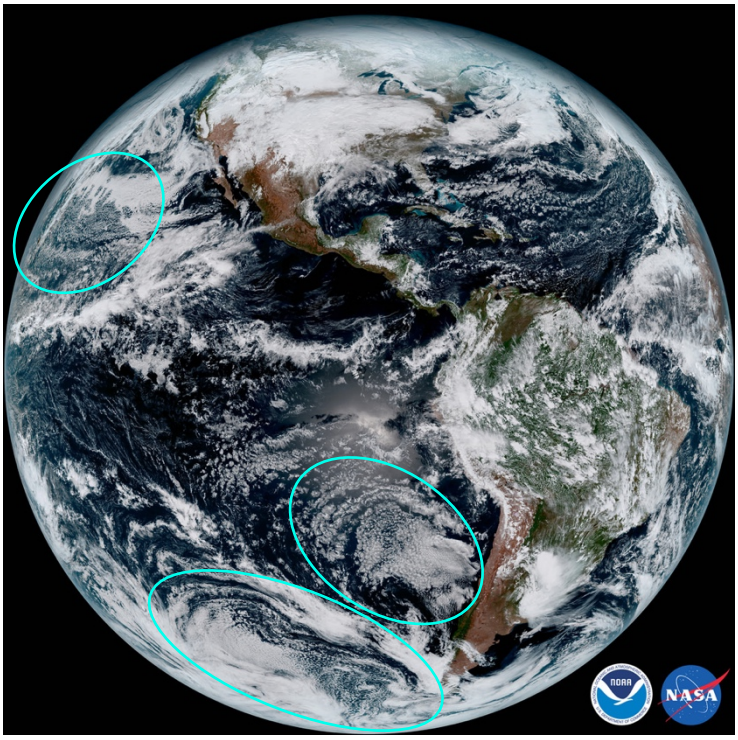

Figure 2 Visual imagery from NASA and NOAA's GOES 16 satellite (January 15, 2017) [Leslie, 2017]. Cyan circles indicate occurrences of open and closed MCC off the west coast of S. America and California and in a cold air outbreak from Antarctica. Closed MCC are nearer to the coast and in the left quadrant of the outbreak before transitioning to open MCC further from the coast and equatorward.

178 from overcast stratocumulus to deeper, broken clouds have been observed in MCAO, consistent
179 with the advection mechanism [*J K Fletcher et al.*, 2016b; *Abel et al.*, 2017 (in press)]. Examples
180 of open and closed MCC can be seen in the satellite imagery from the National Oceanic and
181 Atmospheric Administration (NOAA) and National Aeronautical and Space Administration
182 (NASA) GOES-16 satellite imagery in Figure 2. Classic transitions from open to closed MCC
183 are seen off South America and in an MCAO from the Antarctic. The relative influence of
184 precipitation and advection in these transitions is an open question as these mechanisms tend to
185 occur together in varying degrees, making it difficult to distinguish the primary driver of open
186 MCC formation.

187 The objective of this paper is to develop a predictive metric for MCC clouds using our
188 knowledge of meteorological and thermodynamic influences in the development of these clouds.
189 It is important to note that prior work has found rather small differences in meteorology (i.e.
190 lower tropospheric stability, vertical velocity at 850hPa, and temperature advection) between
191 open and closed MCC in the sub-tropics [*Wood and Hartmann*, 2006]. This suggests that there
192 may be a zonal difference in the importance of these mechanisms. The lack of meteorological
193 differences may also be explained if the differences driving transitions occur upstream of the
194 transition of closed MCC and development of open MCC and disappear later. In this study, we
195 examine the meteorology differences globally, especially focusing on the development of open
196 and closed MCC in the mid- and high-latitudes where MCAO and cyclones dominate. Although
197 the precipitation mechanism is not investigated in detail, understanding where meteorology plays
198 a dominant role will be enlightening for determining the regionality of the mechanisms. Having
199 an MCC predictive metric helps to evaluate parametrizations of these clouds in weather and
200 climate models, which both have considerable cloud related biases [*J Fletcher et al.*, 2016a]. As

201 the impacts of these biases are radiative as well as structural [*Field et al.*, 2011; *Bodas-Salcedo et*
202 *al.*, 2012; *Williams et al.*, 2013], the radiative properties of MCC were motivational for our
203 work. The earlier work of *Muhlbauer et al.* [2014] on these properties is expanded upon. With a
204 better understanding of the radiative characteristics of open and closed MCC and their
205 connection to MCAOs and cyclone cold sectors, we hope to make the sundry model biases more
206 tractable.

207 In section 2, the data and methodology will be discussed. The MCC identifications,
208 reanalysis and satellite data, and the predictive metrics are all detailed here. Three
209 meteorological control metrics are examined: estimated inversion strength, sea-air temperature
210 difference, and an index for marine cold air outbreaks. Section 3 presents the results. In section
211 3.1 we introduce cloud fraction-albedo relationships for open and closed MCC. Section 3.2 is a
212 discussion of the MCC seasonal cycle and what that suggests about the dynamical predictors of
213 cloud morphology. Section 3.3 quantifies the relationships between MCC and the predictor
214 variables on synoptic scales. In section 3.4 we look at MCC composites around cold air
215 outbreaks and what this says about closed to open MCC transitions. We conclude with a
216 summary and discussion of our results and their implications in section 4.

217

218 **2 Data and Methodology**

219 2.1 Mesoscale Cellular Convection Identification

220 MCC types are classified using the *Wood and Hartmann* [2006] neural network algorithm
221 (NNA) applied to a full year of remotely-sensed data in 2008. The essential elements of the NNA
222 and analysis process are briefly described below, see *Wood and Hartmann* [2006] for complete
223 details. This dataset was also utilized in *Muhlbauer et al.* [2014]. The NNA analyzes sub-scenes

224 of retrievals from the National Aeronautic and Space Administration (NASA) Moderate Imaging
225 Sounder (MODIS) *Aqua* satellite to determine cloud morphology [*Platnick et al.*, 2003]. Sub-
226 scenes of the MODIS swath are 256x256 km^2 in size (oversampled by 128 km in each direction).
227 Liquid water path (LWP) of each sub-scene, derived from cloud optical depth (τ) and effective
228 radius (R_{eff}) retrievals, is used to classify low cloud occurrences into the four morphology types
229 discussed in the introduction: open MCC, closed MCC, homogeneous or no MCC, and cellular
230 but disorganized (Figure 1). The probability density function (PDF) and power spectrum of the
231 LWP in each sub-scene is calculated and used as inputs for the three-layer, back-propagating
232 NNA. The use of both the PDF (a one-point statistic) and the power spectrum (a two-point
233 statistic) of LWP is important for accurate cellular morphology identifications. The PDF
234 describes the amount of liquid present and its homogeneity in the clouds. The power spectrum
235 describes the spatial distribution of the LWP in the sub-scene (i.e. the clouds), clearly marking
236 the cellularity of MCC and contributing a higher order statistic to the analysis. Open MCC have
237 strongly skewed LWP PDFs and more high frequency variance of LWP, making the PDF and
238 power spectrum apt identifiers of this kind of MCC [*Wood and Hartmann*, 2006]. The NNA was
239 previously trained and tested on 1000 previously human-identified cloud sub-scenes, split
240 randomly into a testing and a training group. It has an 85-90% success rate in accurately
241 classifying sub-scenes into the four morphological types. Cases that are harder for the human
242 observer to identify (i.e. those cloud sub-scenes that have features similar to more than one
243 morphological type) account for many of the misidentifications [*Wood and Hartmann*, 2006].
244 In our study, the NNA is applied to MODIS *Aqua* Collection 5.1 Level 2 cloud product for
245 all marine data from 65°N to 65°S in 2008. The power spectrum analysis in the NNA requires
246 the clouds to be complete spatially. The NNA was trained on an earlier collection of MODIS

where pixels on cloud edges were not systematically removed from the cloud product retrieval [*King et al.*, 2003; *Platnick et al.*, 2003; *Wood and Hartmann*, 2006]. For consistency, the same method is applied for collection 5.1. Missing cloudy pixels are filled in the sub-scene through a LWP approximation that uses the retrieved LWP and the visual reflectance. A second order polynomial fit of visible reflectance to the log of optical depth is developed from the retrieved pixels in the sub-scene. This fit is then used to compute optical depth for all the pixels in the sub-scene that have not been retrieved but are considered cloudy according to the MOD35 cloud mask [*Ackerman S. A.*, 2002; *King et al.*, 2003]. Cloud droplet number concentration (N_d) is derived for the retrieved cloud pixels using the method of *Bennartz* [2007] and assuming adiabaticity of unity. The non-retrieved cloud pixels are assumed to have N_d equal to the median N_d of the retrieved pixels. Finally, the LWP of the missing pixels in the sub-scene is computed from N_d and τ using the equation [*Wood*, 2006; *Grosvenor and Wood*, 2014]:

$$LWP = \frac{1}{2}\left(\frac{\Gamma_{ad}\tau^6}{A^2k^2N_d^2}\right)^{1/5} \propto \left(\frac{\Gamma_{ad}\tau^6}{N_d^2}\right)^{1/5} \qquad Eq.\ 1$$

where A~0.0145 and k~0.8 are constants and $\Gamma_{ad} = \Gamma_{ad}(T,p)$ is the adiabatic rate of increase of liquid water content with respect to height. All instances of LWP less than equal to 5 g/m^2 are assumed to be clear sky. Thus, the complete LWP used in the NNA consists of the retrieved pixels and the broken and edge pixels that have been filled in though this method. The cloud fraction for a sub-scene is from the MOD35 cloud mask rather than the MOD06 retrieved cloud fraction [*Ackerman S. A.*, 2002]. In the original NNA in *Wood and Hartmann* [2006], only sub-scenes with cloud top temperatures above 273 K were considered usable, low cloud cases [*Ma et al.*, 2000]. The restriction has been modified in this analysis to sub-scene cloud tops being within 30°C of the surface temperature, allowing classification of higher latitude low clouds that have

cooler cloud top temperatures and for the possibility of clouds with larger sea-air temperature differences. Sub-scenes are still restricted to having liquid cloud tops, however, which in combination with the cloud top temperature aims to ensure no ice-topped cloud is analyzed. Many of the higher latitude cloud with liquid tops are super cooled and these may be mixed phase lower down in the cloud [*Field et al.*, 2014; *Abel et al.*, 2017 (in press)]. Thus, the microphysical characteristics of the higher latitude clouds classified by the NNA could be substantially different from the more tropical clouds.

Quality screening was applied to the identification data before analysis. This included land and sea-ice masking. The sea-ice mask was generated based on monthly mean ice concentrations from the National Oceanic and Atmospheric Administration (NOAA) Optimum Interpolation (OI) Sea Surface Temperature (SST) V2 dataset from NOAA/OAR/ESRL PSD [*Reynolds et al.*, 2002]. Regions with monthly ice concentrations larger than 1% were masked out to obtain only the instances of cloud over water. In addition, regions where fewer than 50 occurrence data points (binned into 2.5°x2.5° boxes) occurred over the year were excluded. The maximum number of points was ~500 in any given box. This insured that enough classifications were made in any given area for the results to be representative of the region over the entire annual cycle. In total, there are ~800,000 sub-scenes globally and ~200,000 occurring between 60°S-40°S.

There are several neural network algorithms to classify open and closed MCC other than the one used in *Wood and Hartmann* [2006]. *Gufan et al.* [2016] developed an alternative machine learning system and applied it to satellite observations of clouds previously identified as containing good cases of cellular morphology, an imagery analysis treatment of Geostationary Operational Environmental Satellite (GOES) data. Recent success has been achieved in morphology identification using PDFs of characteristic variables [*Yamaguchi and Feingold*,

292 2015]. Their simpler methodology, which does not use the additional spectral analysis of *Wood*
293 *and Hartmann* [2006], is designed to capture the closed to open cell transition and utilizes liquid
294 water path, droplet number, and optical depth distribution modes and mode indexes as they
295 evolve in time. While effective, this simpler methodology has only been demonstrated on
296 idealized LES simulation and not applied to observational data yet. The NNA from *Wood and*
297 *Hartmann* [2006] remains the most applicable for the MODIS analysis presented here.
298
299 2.2 Reanalysis and satellite data
300 Reanalysis data are employed in this study to examine the large-scale meteorological and
301 thermodynamic influences on cloud development. We used the European Center for Medium-
302 Range Weather Forecasting (ECMWF) ERA-Interim dataset [*Dee et al.*, 2011]. Four times daily
303 data gridded to 1°x1° bins are used in the latitude range 65°N to 65°S for the full year of 2008.
304 Reanalysis data are then collocated with the MCC identifications by linearly interpolating the
305 binned data to the individual identification points in space and time. The collocated reanalysis
306 data, which are associated with the center of the sub-scene at the time of occurrence, is used to
307 compute the meteorological controls (next section) associated with the NNA classifications.
308 Additionally, we utilized the Clouds and the Earth's Radiant Energy System (CERES)
309 satellite data [*Wielicki et al.*, 1996] to examine the radiative effect of the MCC clouds. Retrieved
310 top of atmosphere shortwave flux and solar insolation from the Level 2 SSF Edition 4
311 Instantaneous footprints are used to calculate the instantaneous shortwave albedo [*Wielicki et al.*,
312 1996]. CERES follows closely behind MODIS *Aqua* in the A-train constellation so the data is
313 temporally well-collocated. To spatially collocate the CERES and MODIS identification data,
314 CERES pixels (~25 km circles) are sampled in a circle of 128 km radius centered on the middle

315 of each of the square MCC identification sub-scenes (256x256 km^2). This is similar to the
316 method in *Muhlbauer et al.* [2014] for collocating data products of differing footprints. The
317 albedo over the sampled circle is estimated as the average of the TOA SW flux for the footprints
318 within the MODIS sub-scene divided by the average TOA solar insolation. This albedo includes
319 the clear and cloudy sky associated with the MCC classification. One disadvantage to using the
320 circular average to calculate albedo for the identified sub-scene is that it misses the corners of the
321 sub-scene and any cloud that may be occurring there. The albedo is associated more with the
322 cloud in the center of the sub-scene, which is also what the NNA primarily uses to decide the
323 classifications due to the data windowing [*Wood and Hartmann*, 2006]. However, this will add a
324 systematic bias in comparisons between albedo and any other characteristics derived for the
325 entire sub-scene (i.e. cloud fraction). There will not be more cloud in the corners for a given
326 NNA classification compared to any other type, however, as the sub-scenes used are relatively
327 random samples of cloud fields. One can argue that this bias will only add noise to the
328 comparison and not change the results.
329
330 2.3 Meteorological Control Metrics
331 Three meteorological control metrics are employed in our study, each capturing an aspect
332 of large-scale dynamic and thermodynamic influences on MCC development. They are:
333 estimated inversion strength (EIS), sea-air temperature difference (ΔT), and the marine cold air
334 outbreak index (M) [*Wood and Bretherton*, 2006; *Kolstad and Bracegirdle*, 2008; *J Fletcher et*
335 *al.*, 2016a]. Each is calculated using reanalysis data. EIS is a measure of the strength of the
336 boundary layer inversion, an indicator of the static stability of the lower atmosphere [*Wood and*
337 *Bretherton*, 2006]. It is a correction to the lower-troposphere stability (LTS) metric, originally

introduced in *Klein and Hartmann* [1993], that accounts for tropospheric temperature profile assuming a structure closer to a moist than a dry adiabat and with a result that its gradient is temperature sensitive. *Wood and Bretherton* [2006] found a strong linear relationship between EIS and cloud cover in the key stratocumulus regions across the globe. It has been recently shown that EIS, along with being a good predictor of cloud cover in the relatively quiescent zones such as the Tropics, is a good predictor of cloud cover in dynamically active regions behind cold fronts [*Naud et al.*, 2016]. EIS is calculated as in *Wood and Bretherton* [2006]:

$$EIS = LTS - \Gamma_m^{850}(z_{700} - LCL), LTS = \theta_{700} - \theta_{1000} \qquad Eq.\ 2$$

In this equation, θ_{1000} is the potential temperature of the surface air, LCL is the lifting condensation level, Γ_m^{850} is the moist adiabatic lapse rate at 850 hPa. Surface relative humidity, used in the LCL computation, is approximated as 0.8 in light of its narrow distribution from 60°N to 60°S [*Wood and Bretherton*, 2006]. The second metric, Air-Sea Temperature difference (ΔT), is a symptom of the contrast between the ocean and atmosphere heat content, informative of the energy that could be fluxed from the ocean to atmosphere. This is simply the difference between the surface or skin temperature and the 2-meter temperature:

$$\Delta T = T_{skin} - T_{2m} \qquad Eq.\ 3$$

The final metric tested is the MCAO index (M), originally defined by *Kolstad and Bracegirdle* [2008] and modified by *J Fletcher et al.* [2016a] into temperature units. It is an index effective at identifying occurrences of marine cold air outbreaks. While somewhat similar to LTS (above), it is calculated at different pressure levels and uses the temperature of the sea surface instead of the air at the surface. This emphasizes the extreme temperature contrast between the cold polar air moving above comparatively warmer water, a dynamically favorable condition for planetary boundary layer cloud development. M is defined as:

361 $$M = \theta_{skin} - \theta_{800} \qquad Eq.\ 4$$

362 The effectiveness of these metrics as predictive factors for open and closed MCC is tested in the
363 subsequent section. Examples of M, EIS, and ΔT values with MCC identifications are given in
364 Figure 3, showing a southern hemisphere cold air outbreak and the associated open and closed
365 MCC. The MCAO in this example is roughly a plume of cold air that has moved from the higher
366 latitudes (35°S) to the lower latitudes (20°S). The youngest or strongest part of the MCAO is at
367 the bottom right, coming from the pole. The oldest and weakest part is at the bottom left after it
368 has moved over the ocean counter-clockwise. M (Figure 3c) is the best at following the flow of
369 the cold air outbreak. The static stability, measured by EIS (Figure 3b), is smallest in the young
370 part of the MCAO where the open MCC occur and high in the older air mass where we see the
371 closed MCC. ΔT (Figure 3a) is larger in the young part of the MCAO where the air-sea contrast
372 is largest and smaller in the old part. These signatures are all consistent with our expectations for
373 how open and closed MCC are influenced by meteorology.
374
375 **3 Results**
376 3.1 Cloud fraction – Albedo relations
377 Many studies have demonstrated that fractional cloud cover is a useful quantifier of cloud
378 radiative effect. *D. L. Hartmann and Short* [1980] originally showed the relation between cloud
379 fraction (CF) and albedo and the subsequent cloud impact on radiative balance. More recently,
380 variations in CERES albedo and MODIS cloud fraction were found to be well correlated [*Loeb*
381 *et al.*, 2007]. This suggests that globally, cloud cover anomalies are a good proxy for albedo.
382 From these and other works, we would expect the radiative effect of open and closed MCC to be
383 primarily determined by their CF. Open and closed MCC have overlapping distributions of cloud

384 cover with closed MCC having larger
385 mean CF than open MCC
386 [*Muhlbauer et al.*, 2014]. Where
387 open and closed MCC occur with the
388 same CF, we would expect a similar
389 albedo based on the above logic.
390 Similar cloud fractions in open and
391 closed MCC are very likely to occur
392 as the size of cloud cells, and thus the
393 spread of the large-scale pattern, can
394 change with boundary layer depth
395 and vary across the globe [*Wood and*
396 *Hartmann*, 2006; *Muhlbauer et al.*,
397 2014].

398 Such a qualitative analysis
399 does not consider macrophysics (e.g.
400 liquid water path, LWP) or
401 microphysics (e.g. droplet
402 concentration, N_d) known to be
403 contributing factors to the cloud
404 albedo [*Boers and Mitchell*, 1994;
405 *Wood*, 2006; *George and Wood*,
406 2010]. Indeed, when examined in

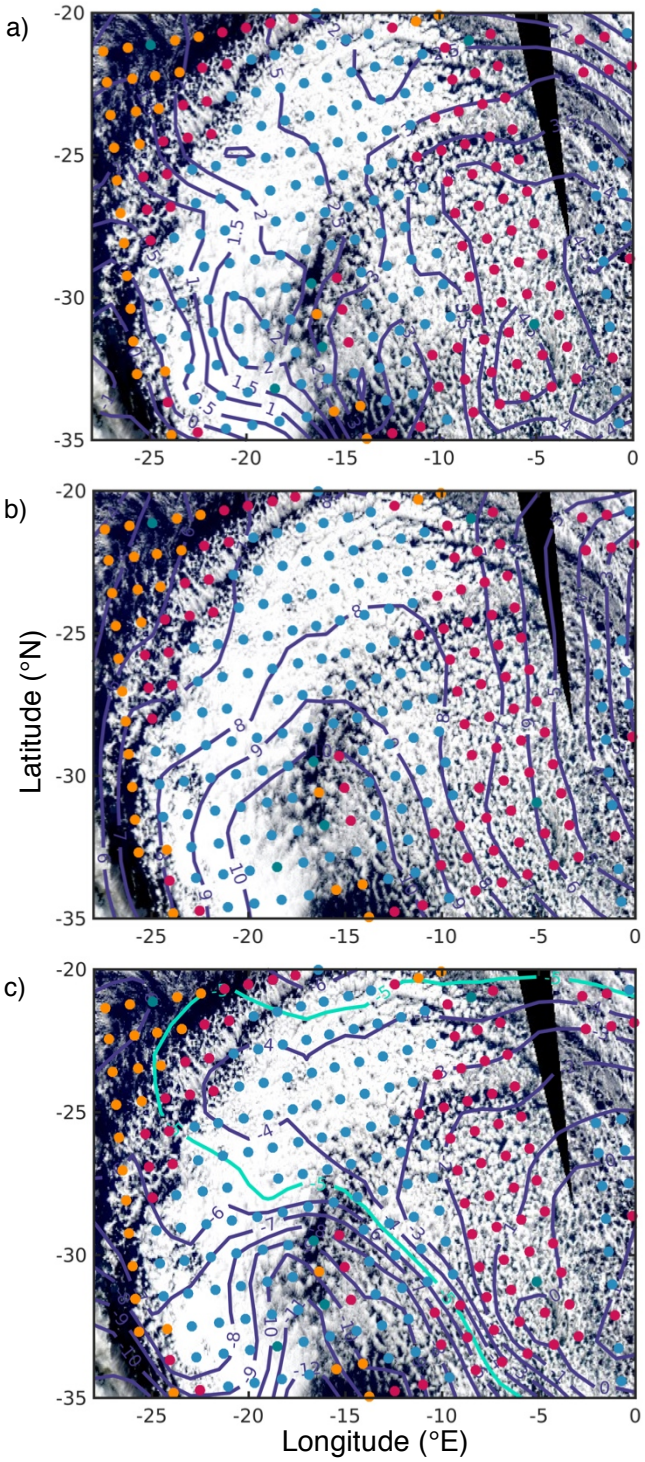

Figure 3 Southern Hemisphere winter (August 13, 2008) case study showing MCC Identifications overlaid on MODIS Aqua surface reflectance with contours of meteorological control metrics: ΔT (a), EIS (b), and M (c) in Kelvin. Identifications are colored by type: closed MCC (blue), open MCC (red), no MCC (green), and cellular but disorganized (yellow). The M= -5 K contour is cyan to indicate what region is strong enough to be considered a MCAO.

PDF form, the microphysical and radiative characteristics of open and closed MCC suggest large differences between types. For example, closed MCC has more frequent light drizzle while open MCC has a higher fraction of heavy drizzle. Closed MCC also tends toward higher shortwave reflectance than open MCC, but the magnitude of reflectance and difference between NNA determined cloud types changes regionally [*Muhlbauer et al.*, 2014]. A technique for quantifying cloud radiative effect while considering the contribution of micro- and macro-physical variations of the cloud is to develop an explicit relationship between the cloud fraction and the cloud albedo [*Webb et al.*, 2001; *F. A. M. Bender et al.*, 2011; *Engstrom et al.*, 2014; *Engstrom et al.*, 2015; *Frida A. M. Bender et al.*, 2016; *F. A. M. Bender et al.*, 2017]. The observed spread in albedo for any fixed cloud fraction will be due primarily to the variability in factors affecting the optical depth of the cloud [*Frida A. M. Bender et al.*, 2016]. Solar zenith angle will affect the albedo as well, particularly in high latitude high cloud fraction cases [*Engstrom et al.*, 2015; *F. A. M. Bender et al.*, 2017]. A correction can be made to remove this influence from the variability but should be kept in mind otherwise [*F. A. M. Bender et al.*, 2017]. A simple separation into cloud types was accomplished in prior analysis by choosing stratocumulus-dominant regions to investigate [*F. A. M. Bender et al.*, 2011; *Engstrom et al.*, 2014; *Frida A. M. Bender et al.*, 2016]. However, these relationships have not been separated based on MCC or cloud morphology explicitly. In future work, we can use these relations to address whether the higher shortwave reflectance of closed MCC is due more to cloud fraction or microphysical and macro-physical reasons.

It is immediately apparent that the CF-albedo relationships are different for open and closed MCC (Figure 4). For a given cloud fraction closed MCC tends to have a higher albedo than open MCC, confirming our suspicion that the albedo of different MCC types is not

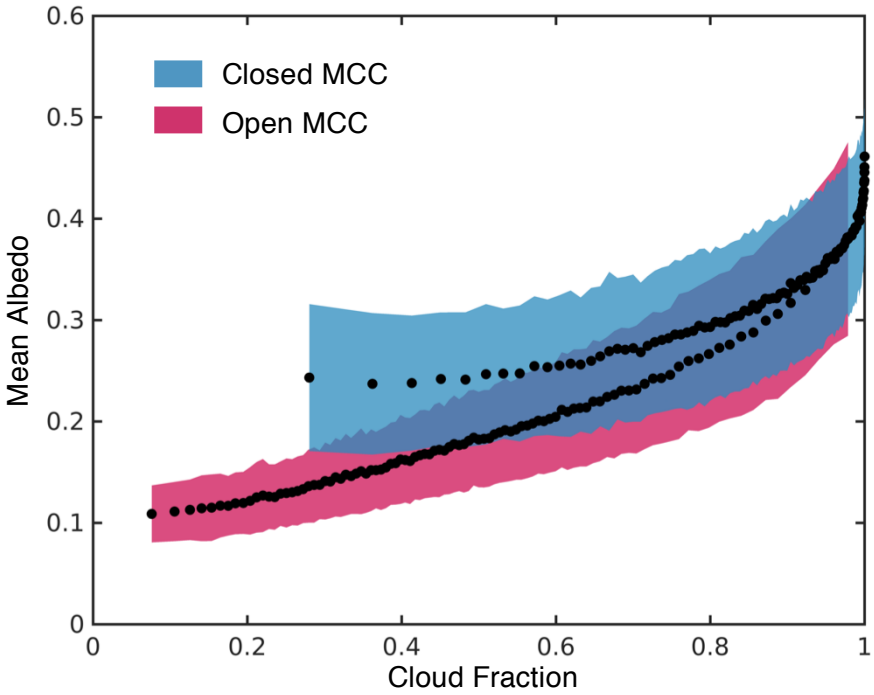

Figure 4 Quantiles of cloud fraction versus sub-scene albedo for open (red) and closed (blue) MCC for 2008 globally (65°S-65°N). Black dots indicate mean albedo within CF quantile bins, variability of data is shown with 1σ shading.

determined by cloud fraction alone. Each cloud type can assume a wide range of cloud fractions. The distribution of albedo around the means partially overlaps between cloud types at higher cloud fractions. However, for cloud fractions between 0.5 and 0.8, both cloud morphologies occur frequently (26% of closed MCC and 34% of open MCC) and are well separated in albedo (by 0.05 on average). What is the potential effect of the albedo difference between open and closed MCC? Assuming typical incoming solar radiation is ~340 W m^{-2}, this 0.05 difference in albedo between types would lead to ~17 W m^{-2} reflected to space dependent on MCC type for the same cloud fraction. Estimating the Southern Ocean shortwave cloud radiative effect as ~-70 W m^{-2} [*Dennis L. Hartmann*, 2016] this is a significant change (~24% change in radiative effect from switching between open and closed MCC excluding the change in CF that could occur).

How do the MCC CF-albedo curves compare to the CF-albedo relationships found for all low clouds [*Webb et al.*, 2001; *F. A. M. Bender et al.*, 2011; *Engstrom et al.*, 2014; *Engstrom et al.*, 2015; *Frida A. M. Bender et al.*, 2016; *F. A. M. Bender et al.*, 2017]? Even though the low

453 cloud relationships are for different time averages (annual and monthly means) than the MCC
454 curves, it is still instructive to compare. Marine low clouds are found to have a quasi-exponential
455 relationship between CF and albedo globally when averaged over a long period (2002-2014)
456 [*Engstrom et al.*, 2015]. While MCC CF-albedo curves have exponential traits as well, the curve
457 shape changes significantly between type and would not be well described by one exponential.
458 Clearly, grouping all low cloud types together results in morphological differences being
459 obscured. This suggests that using a low cloud CF-albedo relationship to evaluate models may
460 have limitations in the eventuality of improved low cloud parameterizations being implemented
461 (particularly if MCC are parametrized). Zonal differences exist in the global low cloud
462 relationships: mid-latitudes contribute to the top of the curve (high CF and high albedo),
463 subtropics to the middle, and tropics to the bottom (lower cloud fraction, lower albedo) [*F. A. M.*
464 *Bender et al.*, 2017]. MCC CF-albedo relationships are broadly consistent, exhibiting similar
465 zonal differences (not shown). The exponential CF-albedo relationship for low clouds indicates
466 that albedo sensitivity to increases in cloud cover increases strongly with cloud fraction
467 [*Engstrom et al.*, 2015; *F. A. M. Bender et al.*, 2017], as seen in other studies [*Webb et al.*, 2001].
468 As the MCC CF-albedo relationships are near-exponential, they will have a similar sensitivity.
469 The sensitivity of open MCC and closed MCC may be different, however, as they are not
470 described by the same exponential and have different rates of increase with CF. There are several
471 interesting possibilities for why there are large differences in albedo between cloud
472 morphologies even for the same CF, but these will be investigated in more detail in subsequent
473 work.
474
475

476 3.2 MCC Climatology

477 The first step to understanding MCC is to observe the location and frequency of their
478 occurrence. *Klein and Hartmann* [1993] established the spatial distribution of low cloud cover
479 and its seasonality but did not distinguish between types of low cloud. *Muhlbauer et al.* [2014]
480 focused on the seasonal frequencies of open, closed, and cellular but disorganized MCC. We
481 expand that work by identifying the magnitude and phase of the seasonal cycle globally for open
482 and closed MCC. Consistent with *Muhlbauer et al.* [2014], a cloud occurrence frequency is
483 defined as the number of times a cloud type (e.g. open MCC) is observed in a region and time
484 period (e.g. over a month) divided by the number of times all NNA-identified cloud types occur
485 in that region and time:

486 $$f_{type}=n_{type}/(n_{open}+ n_{closed} + n_{noMCC} + n_{disorganized}) \qquad Eq.\ 5$$

487 Monthly frequencies were calculated in every 5x5° grid box for open and closed MCC. The
488 annual average of f_{open} (a) and f_{closed} (b) can be seen in Figure 5. Closed MCC are most
489 predominant in the persistent stratocumulus regions marked by the Klein-Hartmann boxes [*Klein*
490 *and Hartmann*, 1993], as previously observed by *Muhlbauer et al.* [2014] and *Atkinson and*
491 *Zhang* [1996]. This is consistent with the idea that closed MCC most commonly occur over cold
492 water to the west of continents, regions of strong stratocumulus decks [*Atkinson and Zhang*,
493 1996]. Open MCC is more uniformly distributed across the globe. A shift from closed to open
494 MCC frequency is seen further west and equatorward of the closed MCC regions, the areas of
495 stratocumulus break-up [*Bretherton and Wyant*, 1997; *Wyant et al.*, 1997; *Yamaguchi and*
496 *Feingold*, 2015]. Cellular but disorganized is the most frequent cloud identified, occurring
497 prominently in the tropics. Clouds without MCC are infrequently observed, the rarest of the four
498 classification types. These last two NNA classification cases do not contain the organized

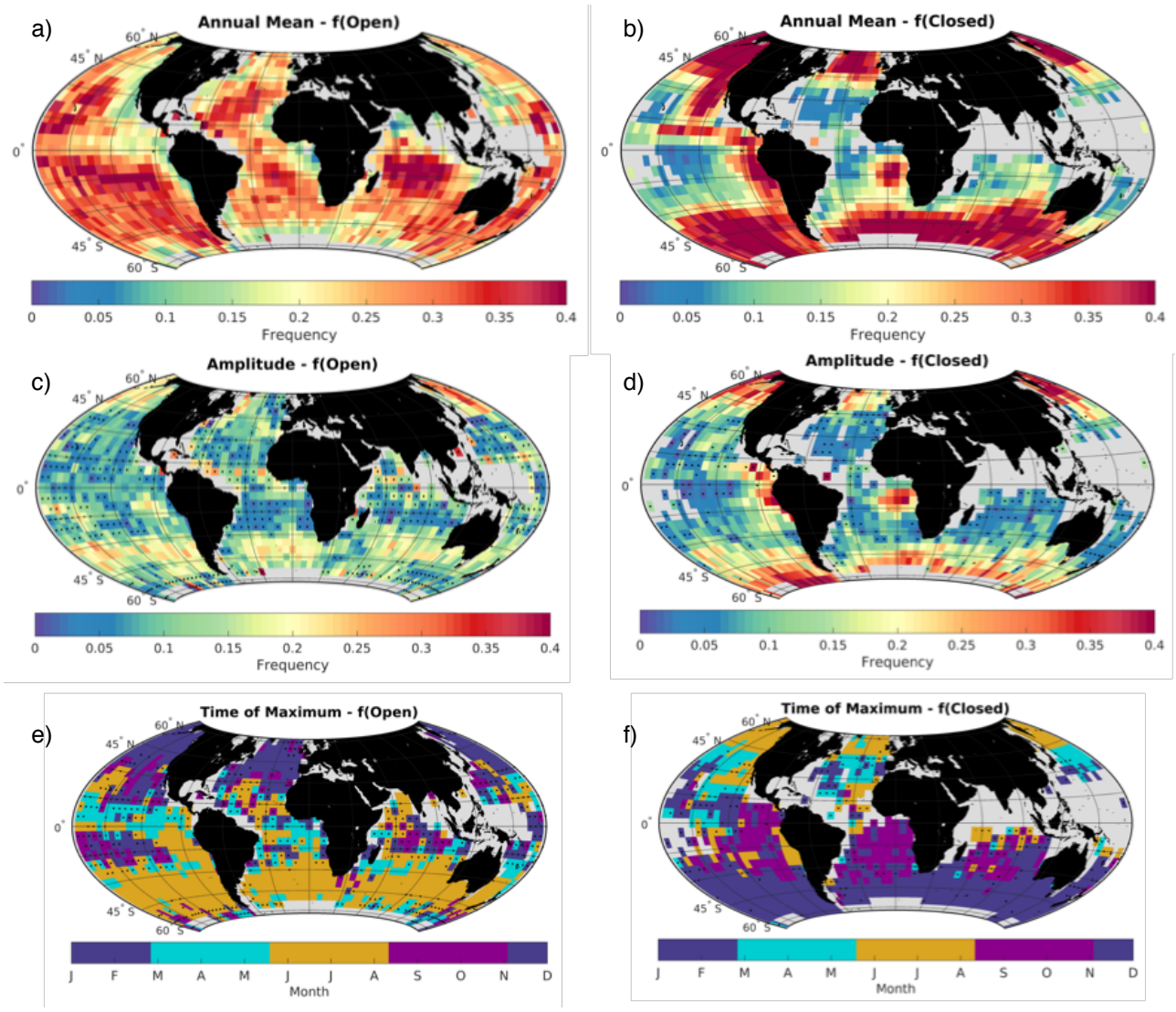

Figure 5 Open (a, c, and e) and closed (b, d, and f) MCC climatologies. Annual mean frequency (a and b) seasonal cycle amplitude (c and d), and month of peak frequency (e and f). Gray areas indicate where there is not enough data retrieved to make an accurate estimate of the frequency. Black dots are where the fit and subsequent results are not significant at a 95% confidence level. Confidence is determined based on a Poisson count method using the number of occurrences.

499 cellular morphology of interest and so will not be discussed further in this analysis. Because of
500 their ubiquity, especially in the mid-latitudes, understanding the forces and controlling
501 meteorology driving open MCC occurrence is important.

502 We examine the seasonal cycle to help determine the meteorological factors in MCC
503 development. A least-squares curve fit sinusoid with a fixed one-year periodicity was applied to
504 the monthly-mean MCC frequencies in each grid box. From this fit we determined the amplitude

505 (half the difference between maximum and minimum) and peak month of cloud occurrence for
506 both types. The MCC seasonal cycle amplitude is shown in (c) and (d) for open and closed
507 MCC, respectively, while the associated month of peak occurrence is shown in (e) and (f) of
508 Figure 5. Closed MCC have the largest seasonal amplitude in the Klein-Hartmann boxes and
509 they peak in the summer of the appropriate hemisphere (June-July-August (JJA) for the Northern
510 Hemisphere (NH), December-January-February (DJF) for the Southern Hemisphere (SH)). The
511 pattern of seasonality and peak month is consistent in the mid-latitudes and becomes more
512 variable and statistically insignificant in the sub-tropics and tropics. Open MCC have the largest
513 seasonal cycle in the mid-latitudes consistent with the observations in *Muhlbauer et al.* [2014].
514 Open MCC exhibit a monthly maximum in occurrence in the hemisphere winter (DJF in NH and
515 JJA in SH). The seasonality and peak month are more varied and less significant in the tropics
516 for open MCC. The ill-defined seasonal pattern of both MCC cloud types in the tropics is not
517 entirely unexpected as the meteorology and dynamics in that area predominantly favor cellular
518 but disorganized clouds [*Muhlbauer et al.*, 2014].

519 The timing and location of the open MCC seasonality is consistent with a strong connection
520 to marine cold air outbreaks. MCAOs occur in the high- and mid-latitudes, with cold air plumes
521 traveling up even into the sub-tropics. They also peak in hemisphere winters. The spatial and
522 temporal parallels between open MCC and MCAOs is in line with earlier theories in the
523 literature [*Agee*, 1987; *Atkinson and Zhang*, 1996; *Wood*, 2012; *Muhlbauer et al.*, 2014]. We will
524 quantify this relationship in the following section.

525

526

527

3.3 MCC Relation to MCAO, EIS, and ΔT

In this section, we compare the seasonal cycles of different cloud morphologies with the seasonal cycles of our three meteorological control variables: EIS, ΔT, and MCAO index (M). First, we compare the monthly frequency of open and closed MCC with ΔT, EIS, and M values averaged over the NH and SH mid-latitude bands (30°-60°N and S, seen in Figure 6). Qualitatively, the seasonal cycle of Open MCC is like that of M (Figure 6c). Closed MCC has nearly the opposite cycle to M (Figure 6c), instead better matching the EIS cycle (Figure 6b). This is observed in both the Northern and Southern Hemispheres. A notable reduction in MCAO magnitude and open MCC frequency occurs in the mid-winter in the Northern Hemisphere. This reduction may be the result of a mid-winter lull in storm activity that can occur in the Pacific basin in the NH at this time [*Nakamura*, 1992]. The tropospheric jet maximizes in winter over the Pacific. When the jet grows too strong, suppression of baroclinic waves will occur and

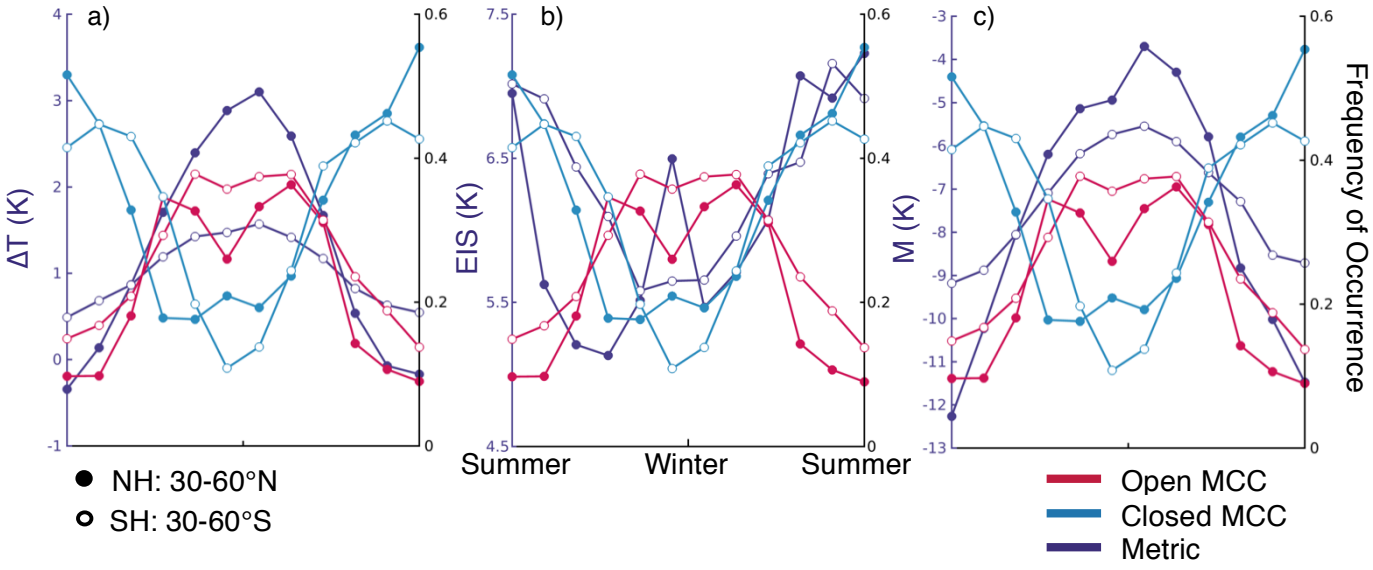

Figure 6 Seasonal cycles of mid-latitude occurrence frequency for open (red) and closed (blue) MCC with the three meteorological control metrics (purple): ΔT (a), EIS (b), and M (c). Seasonal cycles are averaged across northern and southern mid-latitudes (solid dots denote 30-60°N, open circles denote 30-60°S). Seasonality has been shifted to match between the NH and SH (i.e. winter and summer are aligned on the x-axis). Note the lull in M and open MCC frequency and the increase in EIS and closed MCC that occurs in the NH mid-winter.

reduce the meridional flux of heat and zonal momentum [*Nakamura*, 1992]. The mid-winter suppression negatively affects the storminess in the Pacific storm-tracks (i.e. mid-latitude cyclones and associated cold air outbreaks) [*Nakamura*, 1992; *Penny et al.*, 2010]. The mid-winter reduction in M and increase in EIS (Figure 6c and b, respectively) matches expectations for this suppression. The fact that open MCC frequency reduces and closed MCC slightly increases at the same time is encouraging, suggesting that there may be evidence for midwinter suppression in low cloud fields.

Correlation between the MCC seasonal and metric seasonal fits (Figure 7) shows M and EIS meet this expectation the best, respectively, for open and closed MCC correlations. The M-open MCC correlation (Figure *7*e) is large and significant over much of the mid-latitude oceans (where cold air outbreaks occur frequently) [*J Fletcher et al.*, 2016a]. Likewise, the EIS-closed MCC correlation (Figure *7*d) is most positive in the Klein-Hartmann boxes. The consistently robust positive seasonal correlation between M and f_{open}, EIS and f_{closed} suggest that static stability is the best metric for predicting closed MCC seasonality and M is the best for open MCC seasonality.

To explain why M has a strong seasonal cycle correlation with Open MCC and why EIS has a strong seasonal cycle correlation with Closed MCC, we can examine the relations between M, EIS, and ΔT. Recall that M is an estimate of the strength of a cold air outbreak, EIS estimates the static stability, and ΔT estimates the strength of surface heating. M can be written with a few approximations as a function of EIS and ΔT using *Eq. 2*, *3*, and *4*:

$$M = \left(\frac{1000}{p_0}\right)^{R/c_p} \Delta T - EIS - \Gamma_m^{850}(z_{800} - LCL) \sim \Delta T - EIS + const. \qquad Eq.\ 6$$

The relationship between these three metrics is graphically shown with a two-dimensional histogram of M by ΔT and EIS (Figure 8). Each histogram is calculated using a composite of the

MCC identified data for the global, year-long data set. All sub-scenes, from the mid-latitudes, sub-tropics, and tropics are included. The M-ΔT-EIS relationship is shown separately for open and closed MCC but are identical as Eq. 6 shows (Figure 8a and Figure 8c, respectively). In both cases, M depends equally on EIS and ΔT in corroboration with the linear equation derived for M (Eq. 6). We can also see how the frequency of open and closed MCC depend on EIS and ΔT

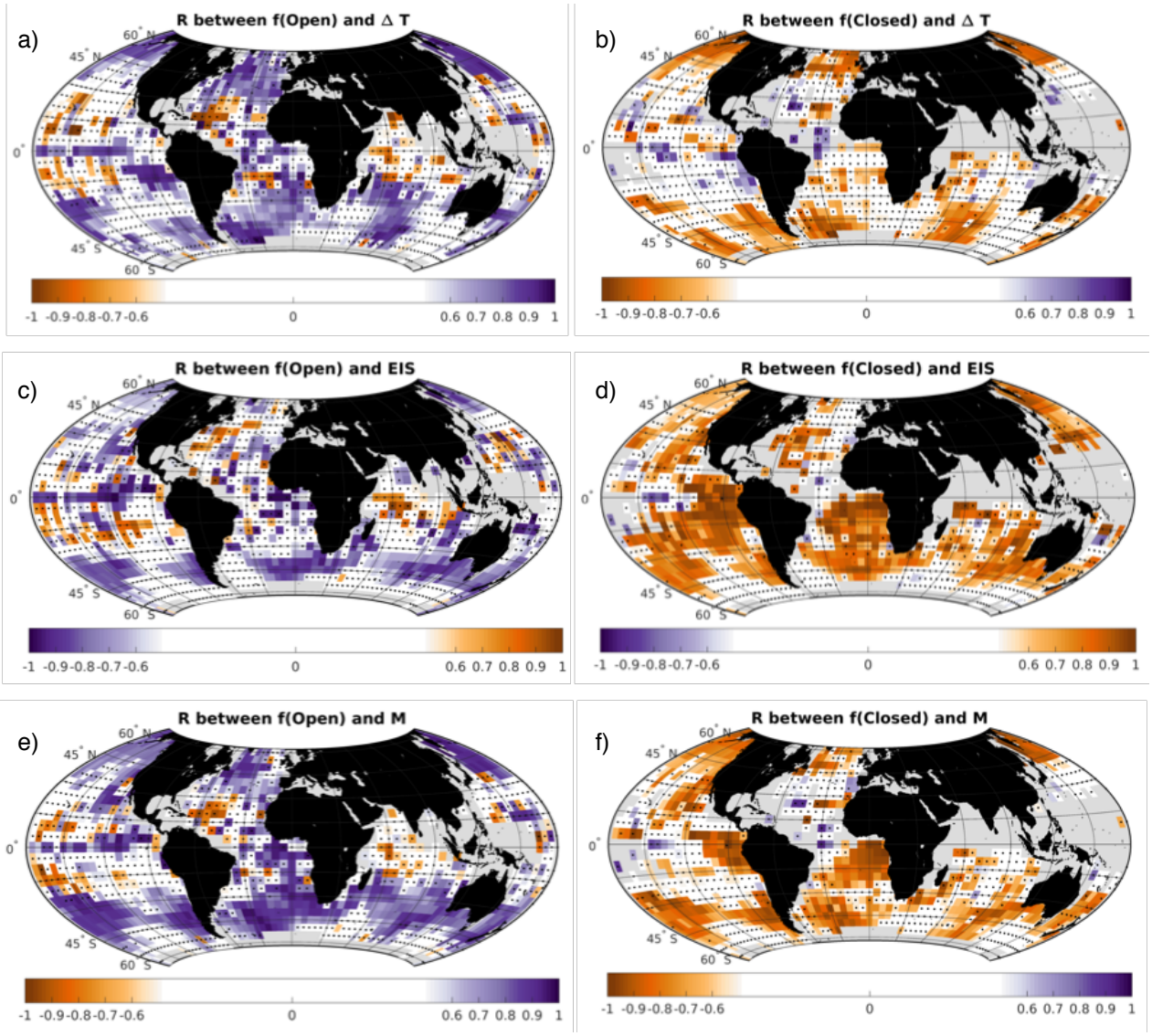

Figure 7 Seasonal cycle correlation coefficients between meteorological control metrics and cloud frequencies. Metrics are ΔT (a and b), EIS (c and d), and MCAO index, M (e and f) while frequencies are f_{open} (a, c, and e) and f_{closed} (a, d, and f). Gray, as before, indicates low data; white is where the correlation is not significant for 12 points (all months); and black dots indicate uncertainty due to other factors.

568 (Figure 8b and Figure 8d). Open MCC occurrence frequency (Figure 8b) mimics the shading of
569 the associated M in Figure 8a, exhibiting an equal dependence on EIS and ΔT. The highest open
570 MCC frequency occurs at the largest M values (i.e. a stronger MCAO). These composites show
571 that both low static stability and strong surface forcing favor open MCC; M can capture both of
572 those factors effectively. Closed MCC (Figure 8d) does not have as close a relation to M (Figure
573 8c) and is more frequent at weaker M, in contrast to open MCC behavior. Closed MCC
574 occurrence frequency (Figure 8d) is quite different from the associated M (Figure 8c), depending
575 more on EIS than ΔT. This is consistent with EIS being the best seasonal predictor for closed

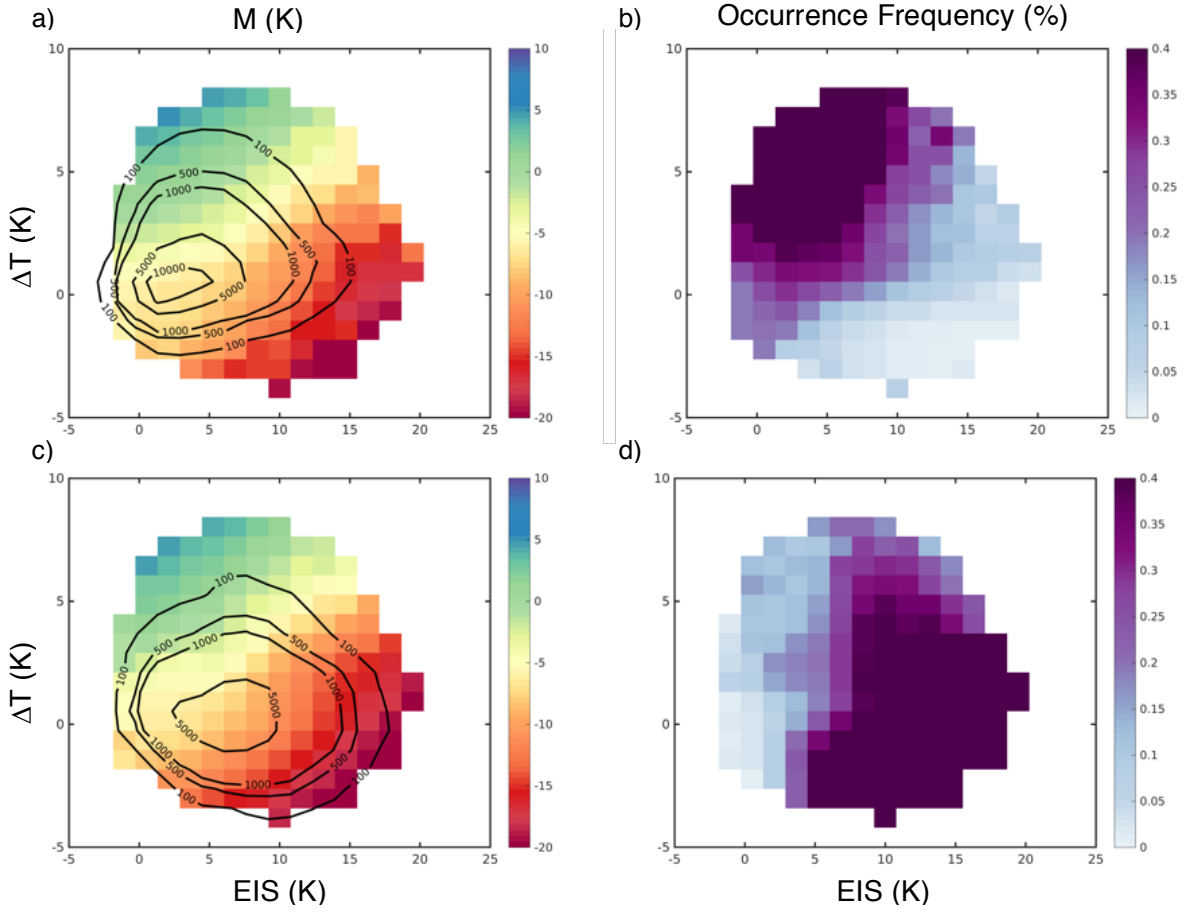

Figure 8 Two dimensional composite histograms of MCAO index and frequency of occurrence for open (a and b) and closed (c and d) MCC. Black contours mark the number of identifications used, indicating the spread in data in the histogram. Note that every box in the histograms is requiered to have at least 50 identifications. Data is for all sub-scenes globally (65°S to 65°N) for 2008.

MCC. Closed MCC also tend to be sustained by longwave cloud-top cooling more than by surface forcing, which may explain the relative lack of closed MCC dependence on ΔT [*Shao and Randall*, 1996; *Wood et al.*, 2011; *Wood*, 2012].

Using the composite data from Figure 8, we can establish a functional dependence of f_{open} and f_{closed} on M (Figure 9). The f_{open} and f_{closed} data binned by EIS and ΔT (Figure 8) are plotted against the similarly binned M in Figure 9 (gray dots). The relationship between M and f_{open} and f_{closed} is well described by a sigmoidal function (green line in Figure 9). The growth curve associated with f_{open} is well correlated to the binned data (R=+0.94) while the decay curve associated with f_{closed} is more weakly correlated (R=-0.83). A weaker correlation for f_{closed} compared to f_{open} is explainable with the above logic (i.e. a stronger dependence on EIS and cloud top cooling than ΔT). Note that composited frequency of occurrence data binned by M alone (purple line with shading for uncertainty in Figure 9) falls within the range of the composited data binned by EIS and ΔT (gray dots). The similarity between the two binning

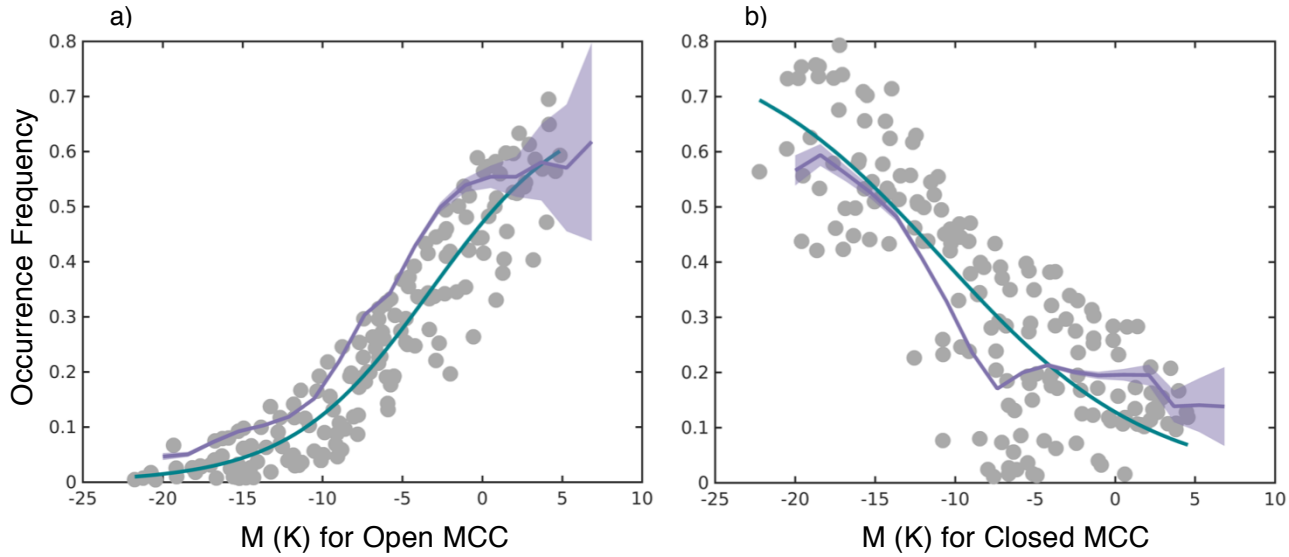

Figure 9 Sigmoidal fits of composited data from Figure 8 *(gray dots) and data binned by M (purple line and shading for 2σ Poisson counting error). Occurrence frequency of open MCC (a) has a strong growth relationship, while the frequency of closed MCC (b) has a weaker decay relationship with M (fit shown as green line).*

methods suggests robustness to the sigmoidal relationships between M and MCC frequency of occurrence.

Is the predictive strength of the M-MCC cloud relationship only due to the strong correlation between the seasonal cycle of cloud occurrence and metric values? We can prove that there is a strong connection on a shorter time scale (i.e. with the seasonal cycle removed) by looking at the monthly PDF median difference between the metric values for open and closed MCC and averaging the differences over the full year (shown in Figure 10a, b, and c respectively for EIS, ΔT, and M). The results show that M is superior to the other metrics tested in distinguishing open and closed MCC on sub-seasonal time-scales. This superiority has two sources: 1) M has the largest separation in value between open and closed MCC and 2) M shows the most grid boxes with statistically significant separation between the average open and closed values as tested by a Wilcoxon rank sum test. All plots are on the same

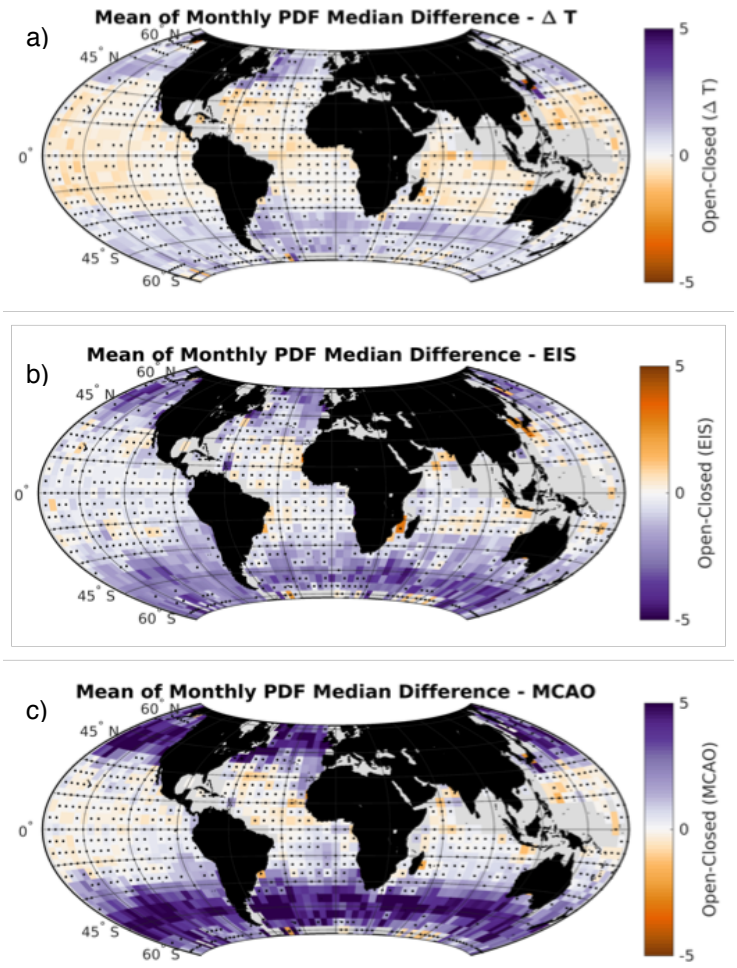

Figure 10 Global maps of the means of monthly differences between the open and closed MCC identified meteorological control metric distribution medians within each grid cell. ΔT (a) has the smallest seperation between average values of open and closed MCC. EIS (b) is larger and has more significant regions. M (c) is the most superior, having the largest seperation and most significant regions of all the metrics tested. Black dots indicate where insignificant at a 95% confidence level as determined by a Wilcoxon rank sum test.

612 temperature scale, -5 to 5 °C, clearly showing the magnitude of separation for each metric. The
613 separation of open and closed MCC identified M values is especially strong and significant in the
614 mid-latitudes. For comparison, for the two latitude bands of 30-60°N and S, there are a total of
615 160 5°x5° grid boxes that are tested to be significant for ΔT (a), 257 for EIS (b), and 332 for M
616 (c). The separation between open and closed values of M is generally not statistically significant
617 over the tropics, which is not unexpected given the differing dynamics there. Interestingly, ΔT
618 has the most statistically significant points in the tropics and the direction of the difference
619 between open and closed MCC clouds switches. We can conclude from the analysis in this
620 section that M is the best of the three metrics at distinguishing between open and closed MCC in
621 latitudes poleward of 30°.
622
623 3.4 Composites of MCAO and MCC environments
624 In the previous sections of this paper, we have shown that the MCAO index, M, is a good
625 predictor of MCC cloud frequency. There is an especially strong relationship of M to open MCC.
626 Thus far we have examined these clouds and their relationships in a static framework, through
627 snapshots of cloud occurrence and associated meteorology. These systems are very dynamic,
628 however, with clouds evolving in time through the influence of MCAO. How well is M able to
629 capture the Lagrangian evolution of these clouds? While the bulk of this question will be
630 answered in subsequent work, a preliminary answer can be found by compositing the MCC
631 occurrence data around MCAO events (Figure 11). Composites of three NNA identification
632 cloud types are shown in Figure 11 for the full year of data and 30°-60°N and S, respectively:
633 closed MCC (a and d), open MCC (b and e), and cellular but disorganized (c and f). MCAO
634 events are identified as contiguous regions having M > -5 K. When compositing around these

635 events, the grid-point where M is a maximum within the closed contour of M > -5 K is chosen as
636 the center MCAO and positioned at the composite origin. The composite-mean location of M=-5
637 K is also shown (dashed line). For reference, composites of sea level pressure are shown as
638 contours as well. Composites of Northern Hemisphere (30°-60°N in a, b, and c) and Southern
639 Hemisphere (30°-60°S in d, e, and f) are shown in Figure 11.

640 Examining the MCC cloud evolution along the mean flow (arrows in Figure 11, as
641 deduced from surface pressure contours) in these composites is a reasonable proxy for

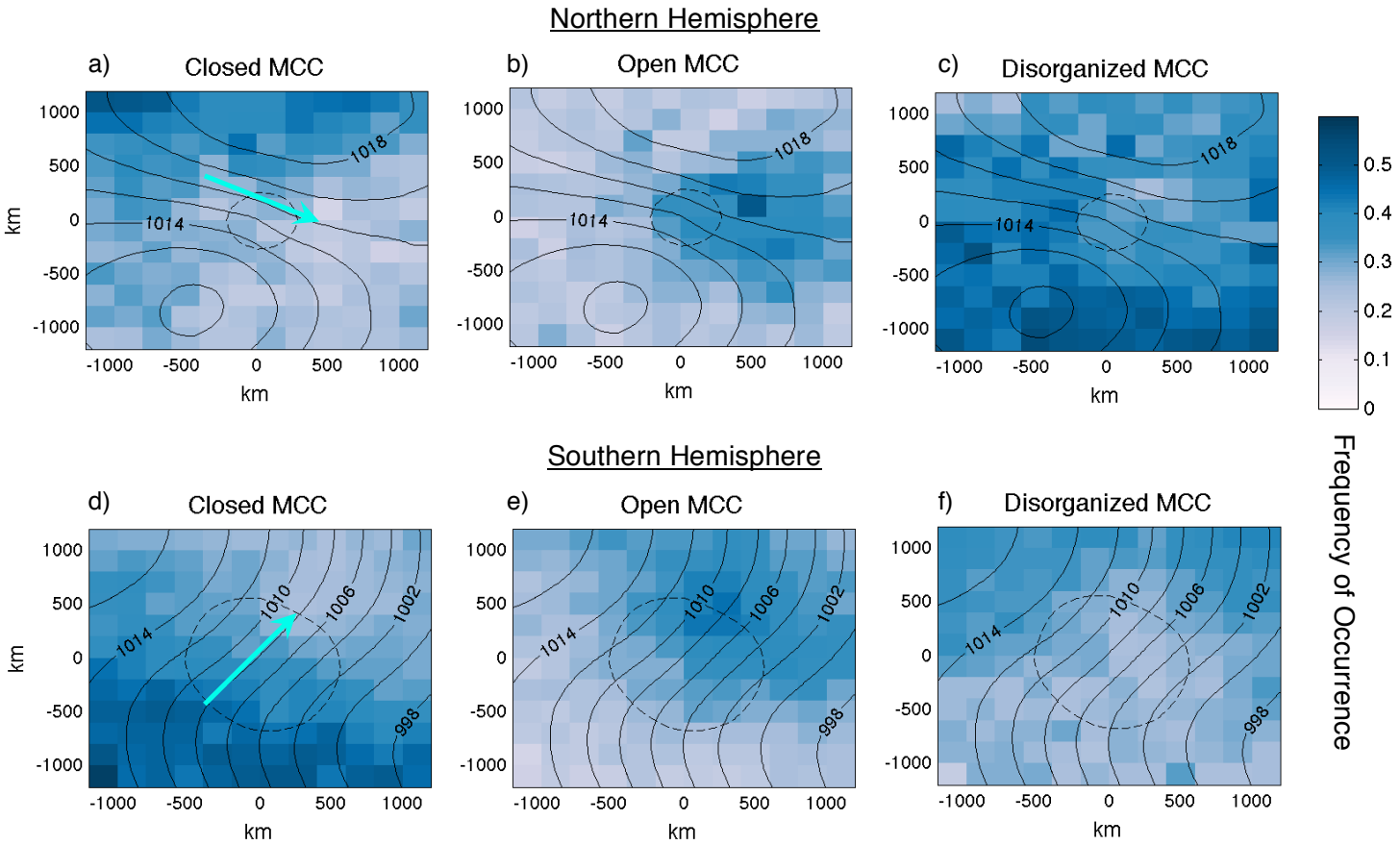

Figure 11 Composites of closed MCC (a, d), open MCC (b, e), and cellular but disorganized (c, f) frequency (color) and sea level pressure (solid contour) around MCAO events. Northern hemisphere (30°-60°N in a, b, c) and southern hemisphere (30°-60°S in d, e, f) composited separately. When an MCAO event is identified, MCC sub-scenes occurring within three hours of the event and within 2000 km of the MCAO center are identified. The location of the MCC sub-scene relative to MCAO center is identified on an equal area grid, and the frequency with which each MCC type occurs in each grid box (bin size 200x200 km) is calculated. M and sea level pressure derived from ERA-Interim are interpolated to an equal area (40x40 km) grid prior to compositing. Times during which an MCAO event is identified, but there is no corresponding MCC sub-scene, are not included in the SLP and M compositing. Cyan arrows indicate mean flow following the SLP contours.

642 Lagrangian evolution of MCC around MCAOs. Note that the SLP contours are not streamlines
643 so this is not the exact time evolution of the clouds but an approximation. High stability over
644 high latitude oceans drives extensive low cloud, frequently of the closed MCC form and
645 occasionally, with the right shearing wind conditions, roll cloud [*Atkinson and Zhang*, 1996; *J*
646 *Fletcher et al.*, 2016a; *J K Fletcher et al.*, 2016b]. The marine cold air outbreak will begin as air
647 over cold SST, heading equatorward over warmer SST and pulling these low clouds with it.
648 Indeed, (a and d) show the highest frequency of closed MCC at the start of the flow (top in a,
649 bottom in d). Note that roll clouds are identified by the NNA as closed MCC, so this includes
650 both cases. The MCAO will advect the clouds over progressively warmer water as it heads to the
651 equator. This results in a transition from closed MCC to open MCC [*Atkinson and Zhang*, 1996;
652 *Wyant et al.*, 1997; *J K Fletcher et al.*, 2016b; *Abel et al.*, 2017 (in press)]. Open MCC are most
653 frequent in the center of the composites in Figure 11, slightly to the east of the mean center of the
654 MCAO event. This is consistent with the flow traced from the SLP contours (diagonal from top
655 left to bottom right in NH, b; bottom left to top right in SH, e). The f_{open} maximum occurs
656 slightly downstream from the peak M values in the Lagrangian perspective, intriguingly. This is
657 consistent with results found in *J Fletcher et al.* [2016a] for composites of ERA-Interim
658 planetary boundary layer (PBL) height around stronger MCAOs (M > 6 K instead of -5 K). They
659 found that a minimum in PBL height occurred far upstream of the M maximum (where closed
660 MCC would occur) and a maximum in PBL height about 200-500 km downstream of the
661 maximum in M (where we see open MCC) [*J Fletcher et al.*, 2016a]. This could be an indication
662 that time is needed for the development of open MCC (i.e. that they need to be advected beyond
663 the peak M that influenced them). Finally, as the flow continues to move the clouds towards the
664 equator, the open MCC will continue to evolve into aggregated cumulus cloud captured by the

665 cellular but disorganized category of the NNA. This growth is seen more clearly in the SH (f) but
666 still exists in the NH (c). A larger amount of cumulus and other disorganized clouds occur in the
667 NH than the SH relative to the other types shown, obscuring the final stage of the transition.
668 These MCAO composites of the MCC show that open and closed MCC are consistently
669 influenced by MCAO events.

670 An intriguing and yet unexplored discovery was made about the environment that open
671 and closed MCC occur within. Along with the meteorological differences illustrated previously,
672 open and closed MCC have very different large-scale vertical velocities (measured in pressure
673 coordinates as ω_{700}, Figure 12a). Zonally averaged annual mean values of ω_{700} are generally
674 more positive for open MCC than closed, indicating larger subsidence in the environment of
675 those clouds. In the subtropics and tropics, open MCC are weakly subsiding or without
676 significant vertical wind. This overlaps with the weakly subsiding or strongly ascending closed
677 MCC seen in those areas. In the mid-latitudes, along with greater subsidence, open MCC have

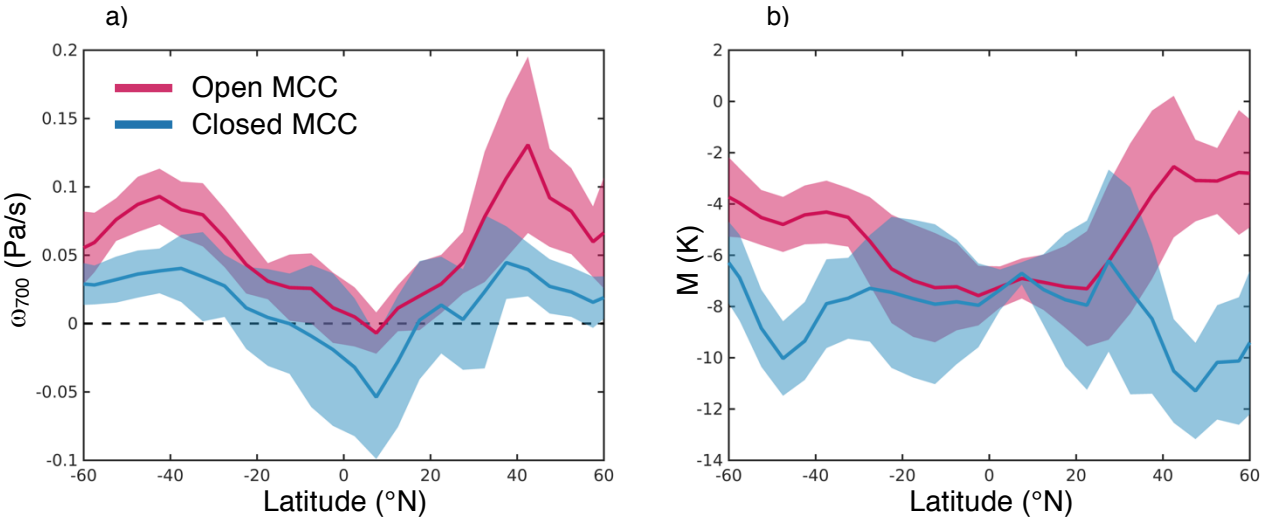

Figure 12 Zonally averaged ω_{700} (a) and M (b) averaged over monthly means (line) with 1σ standard deviation (shading). Open MCC (red) have significantly more subsidence (positive ω_{700}) in the mid-latitudes than closed MCC (blue). M values in the mid-latitudes are also significantly more positive for open than closed.

678 much more positive values of M than closed MCC as we showed earlier in Figure 10. For
679 comparison purposes, M has been shown similar to ω_{700} in Figure 12b. The connection between
680 regions of stronger M values and more subsidence indicates large-scale dynamics at work in
681 MCAO. This is consistent with the descending air, known as the dry intrusion or airstream,
682 typically found on the cold side of cyclones [*Schultz*, 2001; *Field and Wood*, 2007; *Catto*, 2016].
683 It is remarkable that open cells are associated with both weak static stability and strong
684 subsidence. *Berner et al.* [2013] showed that subsidence can suppress transition from closed to
685 open cells, making this finding somewhat counterintuitive and worthy of future explanation. The
686 source of subsidence, mechanics of its influence on open and closed MCC, and the evolution of
687 open and closed MCC with MCAO will be investigated with the help of Lagrangian trajectories
688 in the future.
689

690 **4 Summary and Discussion**

691 We set out to test the hypothesis that the frequency of occurrence of open MCC is
692 strongly tied to cold air outbreaks and that a simple metric can be used to predict MCC
693 occurrence. Three metrics were chosen to represent the key influences on development: M, the
694 marine cold air outbreak index; EIS, estimated inversion strength; and ΔT, sea-air temperature
695 difference.

696 We discovered several important aspects of open and closed MCC structure, radiative
697 impacts, and formation mechanisms. These are as follows:

698 First, open and closed MCC have distinct cloud fraction-albedo relations, indicating that
699 the structure and microphysical properties of open and closed MCC are sufficiently different for
700 a given cloud fraction to impact the optical depth and thus albedo. Closed MCC, for a given

cloud fraction, tends to have a higher albedo than open MCC except at very high cloud fractions. The CF-albedo relationships showed that prediction of open and closed MCC based on cloud fraction alone will be insufficient as it cannot capture the complex MCC morphology.

Second, we described the global nature of open and closed MCC and determined their strong seasonality. Closed MCC occur in the cold Eastern sub-tropical oceans and over summertime mid-latitude oceans while open MCC are widespread globally, as in *Muhlbauer et al.* [2014]. The seasonal cycle of open MCC is best correlated with the MCAO index. A strong connection between outbreaks and open cloud development is found, consistent with the literature [*Agee*, 1987; *Atkinson and Zhang*, 1996; *Wood*, 2012; *Muhlbauer et al.*, 2014]. The seasonal cycle of closed MCC is best correlated with EIS, in line with a stronger influence by longwave cloud top cooling on closed MCC than surface forcing [*Shao and Randall*, 1996].

Third, the superior open MCC predictive ability of M over the other metrics is largely due to its encompassing of surface forcing and low static stability. Surface forcing has been previously established as a driver of open MCC development [*Kazil et al.*, 2014]; we find that low static stability is favorable to open MCC as well. Sigmoidal relations were found between frequency of open and closed MCC and M. M is a slightly inferior predictor for closed MCC because of the cloud type's stronger dependence on EIS over ΔT. Of the metrics tested, M is also the best discriminator between occurrence of open and closed MCC.

Fourth, open and closed MCC evolve with MCAO events. Composites of MCC around MCAO events indicate that MCAO coming from regions of cold SST and off high-latitude ice and land drive a transition from closed to open MCC and then to cellular but disorganized clouds. Mid-latitude and tropical open MCC tend to occur in more strongly subsiding

723 environments than closed MCC. This may be connected to the dynamics of MCAO events and
724 will be investigated in the future using Lagrangian trajectories.

725 Our results have interesting implications for cloud feedbacks. Much of the research on cloud
726 feedbacks and improving model predictions uses fractional cloud cover as a way of quantifying
727 cloud radiative influence. It is highly probable that cloud cover will change with global warming.
728 Metrics like estimated inversion strength (EIS) [*Wood and Bretherton*, 2006] and sea surface
729 temperature (SST) predict low cloud cover in observations of the current climate and in GCM-
730 simulated present and future climates [*Clement et al.*, 2009; *Qu et al.*, 2014; *Myers and Norris*,
731 2015; *Qu et al.*, 2015; *Seethala et al.*, 2015; *Myers and Norris*, 2016; *Norris et al.*, 2016]. The
732 magnitude of change in low cloud cover is still uncertain in GCMs [*Qu et al.*, 2014; *Qu et al.*,
733 2015]. However, they all indicate that cloud cover will reduce with global warming thus
734 constituting a positive feedback. *Kolstad and Bracegirdle* [2008] found that MCAO's in the
735 Northern Hemisphere are predicted to weaken in strength with global warming, although their
736 frequency stays the same. A weakening would yield a reduction in the magnitude of M in the NH
737 and possibly the SH. If our closed and open MCC relations with M (Figure 9) hold in a warmed
738 climate and MCAOs are affected in both hemispheres, this would suggest that in the future there
739 may be less open MCC and more closed MCC in the middle and high latitudes. If we further
740 suppose that the cloud fraction-albedo relations (Figure 4) hold in a warmed climate, this shift to
741 more closed MCC suggests that we would have a shift from lower albedo clouds to higher albedo
742 clouds. This would constitute a negative cloud feedback and would be important given the
743 coverage and frequency of these clouds. A decrease in cloud cover *and* an increase in closed
744 MCC frequency are not mutually exclusive as we have shown that closed MCC exist for a range
745 of cloud fractions. In this instance, we could have more closed MCC clouds (with higher albedo)

746 but lower cloud fraction (consistent with model predictions). The feedback from a shift in MCC
747 type driven by MCAO weakening would change the degree of positive feedback expected from a
748 decrease in cloud cover. MCC clouds can significantly impact the climate system and do not, as-
749 yet, have a well understood behavior under global warming. Determining the influence of
750 MCAO's and the key drivers of MCC, however, can begin to solve that problem.
751

752 **Acknowledgements**

753 The authors acknowledge the Level-1 and Atmosphere Archive & Distribution System (LAADS)
754 Distributed Active Archive Center (DAAC) for NASA MODIS data used in the neural network
755 and the NASA Langley Research Center Atmospheric Science Data Center (ASDC) for CERES
756 data. The authors also thank Ryan Eastman for providing ECMWF ERA-Interim Reanalysis data
757 and insight. Additionally, the authors wish to acknowledge the invaluable discussions and
758 support of Daniel McCoy, Chris Bretherton, and Kuan-Ting O. McCoy acknowledges funding
759 for this work from the American Meteorological Society Graduate Fellowship and the National
760 Science Foundation Graduate Fellowship Program (Grant: DGE-1256082). Additional funding
761 was provided by NASA Award NNX13AQ35G.
762

763 **References**
764
765 Abel, S. J., I. A. Boutle, K. Waite, S. Fox, P. R. A. Brown, R. J. Cotton, G. Lloyd, T. W. Choularton, and
766 K. N. Bower (2017 (in press)), The role of precipitation in controlling the transition from
767 stratocumulus to cumulus clouds in a northern hemisphere cold air outbreak, *Journal of the*
768 *Atmospheric Sciences*.
769 Ackerman S. A., a. C. (2002), Discriminating Clear-Sky from Cloud with MODIS Algorithm Theoretical
770 Basis Document (MOD35)*Rep.*, NASA.
771 Agee, E. M. (1984), OBSERVATIONS FROM SPACE AND THERMAL-CONVECTION - A
772 HISTORICAL-PERSPECTIVE, *Bulletin of the American Meteorological Society*, *65*(9), 938-949,
773 doi:10.1175/1520-0477(1984)065<0938:ofsatc>2.0.co;2.
774 Agee, E. M. (1987), MESOSCALE CELLULAR CONVECTION OVER THE OCEANS, *Dyn. Atmos.*
775 *Oceans*, *10*(4), 317-341, doi:10.1016/0377-0265(87)90023-6.
776 Agee, E. M., T. S. Chen, and K. E. Dowell (1973), REVIEW OF MESOSCALE CELLULAR
777 CONVECTION, *Bulletin of the American Meteorological Society*, *54*(10), 1004-1012,
778 doi:10.1175/1520-0477(1973)054<1004:aromcc>2.0.co;2.
779 Atkinson, B. W., and J. W. Zhang (1996), Mesoscale shallow convection in the atmosphere, *Reviews of*
780 *Geophysics*, *34*(4), 403-431, doi:10.1029/96rg02623.
781 Bénard, H. (1901), Les tourbillons cellulaires dans une nappe liquide. - Méthodes optiques d'observation
782 et d'enregistrement, *J. Phys. Theor. Appl.*, *10*(1), 254-266.
783 Bender, F. A. M., R. J. Charlson, A. M. L. Ekman, and L. V. Leahy (2011), Quantification of Monthly
784 Mean Regional-Scale Albedo of Marine Stratiform Clouds in Satellite Observations and GCMs,
785 *Journal of Applied Meteorology and Climatology*, *50*(10), 2139-2148, doi:10.1175/jamc-d-11-049.1.
786 Bender, F. A. M., A. Engstroem, R. Wood, and R. J. Charlson (2017), Evaluation of hemispheric
787 asymmetries in marine cloud radiative properties, *Journal of Climate*
788 Bender, F. A. M., A. Engstrom, and J. Karlsson (2016), Factors Controlling Cloud Albedo in Marine
789 Subtropical Stratocumulus Regions in Climate Models and Satellite Observations, *Journal of*
790 *Climate*, *29*(10), 3559-3587, doi:10.1175/jcli-d-15-0095.1.
791 Bennartz, R. (2007), Global assessment of marine boundary layer cloud droplet number concentration
792 from satellite, *Journal of Geophysical Research*, *112*(D2), doi:10.1029/2006jd007547.
793 Bennartz, R., M. D. Shupe, D. D. Turner, V. P. Walden, K. Steffen, C. J. Cox, M. S. Kulie, N. B. Miller,
794 and C. Pettersen (2013), July 2012 Greenland melt extent enhanced by low-level liquid clouds,
795 *Nature*, *496*(7443), 83-86,
796 doi:http://www.nature.com/nature/journal/v496/n7443/abs/nature12002.html - supplementary-
797 information.
798 Berner, A. H., C. S. Bretherton, R. Wood, and A. Muhlbauer (2013), Marine boundary layer cloud
799 regimes and POC formation in a CRM coupled to a bulk aerosol scheme, *Atmospheric Chemistry and*
800 *Physics*, *13*(24), 12549-12572, doi:10.5194/acp-13-12549-2013.
801 Bodas-Salcedo, A., P. G. Hill, K. Furtado, K. D. Williams, P. R. Field, J. C. Manners, and P. Hyder
802 (2016), Large Contribution of Supercooled Liquid Clouds to the Solar Radiation Budget of the
803 Southern Ocean, *Journal of Climate*, *29*(11), 4213-4228, doi:10.1175/jcli-d-15-0564.1.
804 Bodas-Salcedo, A., K. D. Williams, P. R. Field, and A. P. Lock (2012), The Surface Downwelling Solar
805 Radiation Surplus over the Southern Ocean in the Met Office Model: The Role of Midlatitude
806 Cyclone Clouds, *Journal of Climate*, *25*(21), 7467-7486, doi:10.1175/jcli-d-11-00702.1.
807 Boers, R., and R. M. Mitchell (1994), Absorption feedback in stratocumulus clouds Influence on cloud
808 top albedo, *Tellus A*, *46*(3), 229-241, doi:10.1034/j.1600-0870.1994.00001.x.
809 Boucher, O., D. Randall, P. Artaxo, C. Bretherton, G. Feingold, P. Forster, V.-M. Kerminen, Y. Kondo,
810 H. Liao, U. Lohmann, P. Rasch, S.K. Satheesh, S. Sherwood, B. Stevens and X.Y. Zhang, (2013),
811 Clouds and Aerosols*Rep.*, Cambridge University Press, Cambridge, United Kingdom and New York,
812 NY, USA.

Bretherton, C. S., and M. C. Wyant (1997), Moisture Transport, Lower-Tropospheric Stability, and Decoupling of Cloud-Topped Boundary Layers, *Journal of the Atmospheric Sciences*, *54*(1), 148-167, doi:10.1175/1520-0469(1997)054<0148:mtltsa>2.0.co;2.

Brummer, B. (1996), Boundary-layer modification in wintertime cold-air outbreaks from the arctic sea ice, *Boundary-Layer Meteorology*, *80*(1-2), 109-125, doi:10.1007/bf00119014.

Catto, J. L. (2016), Extratropical cyclone classification and its use in climate studies, *Reviews of Geophysics*, doi:10.1002/2016rg000519.

Clement, A. C., R. Burgman, and J. R. Norris (2009), Observational and Model Evidence for Positive Low-Level Cloud Feedback, *Science*, *325*(5939), 460-464, doi:10.1126/science.1171255.

Dee, D. P., et al. (2011), The ERA-Interim reanalysis: configuration and performance of the data assimilation system, *Quarterly Journal of the Royal Meteorological Society*, *137*(656), 553-597, doi:10.1002/qj.828.

Engstrom, A., F. A. M. Bender, R. J. Charlson, and R. Wood (2015), The nonlinear relationship between albedo and cloud fraction on near-global, monthly mean scale in observations and in the CMIP5 model ensemble, *Geophysical Research Letters*, *42*(21), 9571-9578, doi:10.1002/2015gl066275.

Engstrom, A., F. A. M. Bender, and J. Karlsson (2014), Improved Representation of Marine Stratocumulus Cloud Shortwave Radiative Properties in the CMIP5 Climate Models, *Journal of Climate*, *27*(16), 6175-6188, doi:10.1175/jcli-d-13-00755.1.

Feingold, G., I. Koren, H. Wang, H. Xue, and W. A. Brewer (2010), Precipitation-generated oscillations in open cellular cloud fields, *Nature*, *466*(7308), 849-852, doi:http://www.nature.com/nature/journal/v466/n7308/abs/nature09314.html - supplementary-information.

Field, P. R., A. Bodas-Salcedo, and M. E. Brooks (2011), Using model analysis and satellite data to assess cloud and precipitation in midlatitude cyclones, *Quarterly Journal of the Royal Meteorological Society*, *137*(659), 1501-1515, doi:10.1002/qj.858.

Field, P. R., R. J. Cotton, K. McBeath, A. P. Lock, S. Webster, and R. P. Allan (2014), Improving a convection-permitting model simulation of a cold air outbreak, *Quarterly Journal of the Royal Meteorological Society*, *140*(678), 124-138, doi:10.1002/qj.2116.

Field, P. R., and R. Wood (2007), Precipitation and cloud structure in midlatitude cyclones, *Journal of Climate*, *20*(2), 233-254, doi:10.1175/jcli3998.1.

Fletcher, J., S. Mason, and C. Jakob (2016a), The Climatology, Meteorology, and Boundary Layer Structure of Marine Cold Air Outbreaks in Both Hemispheres*, *Journal of Climate*, *29*(6), 1999-2014, doi:10.1175/jcli-d-15-0268.1.

Fletcher, J. K., S. Mason, and C. Jakob (2016b), A Climatology of Clouds in Marine Cold Air Outbreaks in Both Hemispheres, *Journal of Climate*, *29*(18), 6677-6692, doi:10.1175/jcli-d-15-0783.1.

Forbes, R. M., and M. Ahlgrimm (2014), On the Representation of High-Latitude Boundary Layer Mixed-Phase Cloud in the ECMWF Global Model, *Monthly Weather Review*, *142*(9), 3425-3445, doi:10.1175/mwr-d-13-00325.1.

George, R. C., and R. Wood (2010), Subseasonal variability of low cloud radiative properties over the southeast Pacific Ocean, *Atmospheric Chemistry and Physics*, *10*(8), 4047-4063, doi:10.5194/acp-10-4047-2010.

Grosvenor, D. P., and R. Wood (2014), The effect of solar zenith angle on MODIS cloud optical and microphysical retrievals within marine liquid water clouds, *Atmospheric Chemistry and Physics*, *14*(14), 7291-7321, doi:10.5194/acp-14-7291-2014.

Gufan, A., Y. Lehahn, E. Fredj, C. Price, R. Kurchin, and I. Koren (2016), Segmentation and Tracking of Marine Cellular Clouds observed by Geostationary Satellites, *Int. J. Remote Sens.*, *37*(5), 1055-1068, doi:10.1080/2150704x.2016.1142681.

Hartmann, D. L. (2016), *Global Physical Climatology*, 2 ed., Elsevier.

Hartmann, D. L., and D. A. Short (1980), ON THE USE OF EARTH RADIATION BUDGET STATISTICS FOR STUDIES OF CLOUDS AND CLIMATE, *Journal of the Atmospheric Sciences*, *37*(6), 1233-1250, doi:10.1175/1520-0469(1980)037<1233:otuoer>2.0.co;2.

Kay, J. E., C. Wall, V. Yettella, B. Medeiros, C. Hannay, P. Caldwell, and C. Bitz (2016), Global Climate Impacts of Fixing the Southern Ocean Shortwave Radiation Bias in the Community Earth System Model (CESM), *Journal of Climate*, *29*(12), 4617-4636, doi:10.1175/jcli-d-15-0358.1.

Kazil, J., G. Feingold, H. Wang, and T. Yamaguchi (2014), On the interaction between marine boundary layer cellular cloudiness and surface heat fluxes, *Atmospheric Chemistry and Physics*, *14*(1), 61-79, doi:10.5194/acp-14-61-2014.

King, M. D., W. P. Menzel, Y. J. Kaufman, D. Tanre, B. C. Gao, S. Platnick, S. A. Ackerman, L. A. Remer, R. Pincus, and P. A. Hubanks (2003), Cloud and aerosol properties, precipitable water, and profiles of temperature and water vapor from MODIS, *Ieee Transactions on Geoscience and Remote Sensing*, *41*(2), 442-458, doi:10.1109/tgrs.2002.808226.

Klein, S. A., and D. L. Hartmann (1993), THE SEASONAL CYCLE OF LOW STRATIFORM CLOUDS, *Journal of Climate*, *6*(8), 1587-1606, doi:10.1175/1520-0442(1993)006<1587:tscols>2.0.co;2.

Kolstad, E. W., and T. J. Bracegirdle (2008), Marine cold-air outbreaks in the future: an assessment of IPCC AR4 model results for the Northern Hemisphere, *Climate Dynamics*, *30*(7-8), 871-885, doi:10.1007/s00382-007-0331-0.

Kolstad, E. W., T. J. Bracegirdle, and I. A. Seierstad (2009), Marine cold-air outbreaks in the North Atlantic: temporal distribution and associations with large-scale atmospheric circulation, *Climate Dynamics*, *33*(2-3), 187-197, doi:10.1007/s00382-008-0431-5.

Leslie, J. (2017), NOAA's GOES-16 Satellite Sends First Images to Earth, edited by K. Hille.

Loeb, N. G., B. A. Wielicki, F. G. Rose, and D. R. Doelling (2007), Variability in global top-of-atmosphere shortwave radiation between 2000 and 2005, *Geophysical Research Letters*, *34*(3), n/a-n/a, doi:10.1029/2006GL028196.

Ma, X. L., Z. Wan, C. C. Moeller, W. P. Menzel, L. E. Gumley, and Y. Zhang (2000), Retrieval of geophysical parameters from Moderate Resolution Imaging Spectroradiometer thermal infrared data: evaluation of a two-step physical algorithm, *Applied Optics*, *39*(20), 3537-3550, doi:10.1364/AO.39.003537.

McCoy, D. T., I. Tan, D. L. Hartmann, M. D. Zelinka, and T. Storelvmo (2016), On the relationships among cloud cover, mixed-phase partitioning, and planetary albedo in GCMs, *J. Adv. Model. Earth Syst.*, *8*(2), 650-668, doi:10.1002/2015ms000589.

Morrison, H., G. de Boer, G. Feingold, J. Harrington, M. D. Shupe, and K. Sulia (2012), Resilience of persistent Arctic mixed-phase clouds, *Nature Geosci*, *5*(1), 11-17.

Muhlbauer, A., I. L. McCoy, and R. Wood (2014), Climatology of stratocumulus cloud morphologies: microphysical properties and radiative effects, *Atmospheric Chemistry and Physics*, *14*(13), 6695-6716, doi:10.5194/acp-14-6695-2014.

Muller, G., and A. Chlond (1996), Three-dimensional numerical study of cell broadening during cold-air outbreaks, *Boundary-Layer Meteorology*, *81*(3-4), 289-323, doi:10.1007/bf02430333.

Myers, T. A., and J. R. Norris (2015), On the Relationships between Subtropical Clouds and Meteorology in Observations and CMIP3 and CMIP5 Models, *Journal of Climate*, *28*(8), 2945-2967, doi:10.1175/JCLI-D-14-00475.1.

Myers, T. A., and J. R. Norris (2016), Reducing the uncertainty in subtropical cloud feedback, *Geophys. Res. Lett.*, n/a-n/a, doi:10.1002/2015GL067416.

Nakamura, H. (1992), Midwinter Suppression of Baroclinic Wave Activity in the Pacific, *Journal of the Atmospheric Sciences*, *49*(17), 1629-1642, doi:10.1175/1520-0469(1992)049<1629:MSOBWA>2.0.CO;2.

Naud, C. M., J. F. Booth, and A. D. Del Genio (2014), Evaluation of ERA-Interim and MERRA Cloudiness in the Southern Ocean, *Journal of Climate*, *27*(5), 2109-2124, doi:10.1175/jcli-d-13-00432.1.

Naud, C. M., J. F. Booth, and A. D. Del Genio (2016), The Relationship between Boundary Layer Stability and Cloud Cover in the Post-Cold-Frontal Region, *Journal of Climate*, *29*(22), 8129-8149, doi:10.1175/jcli-d-15-0700.1.

915 Norris, J. R., R. J. Allen, A. T. Evan, M. D. Zelinka, C. W. O'Dell, and S. A. Klein (2016), Evidence for
916 climate change in the satellite cloud record, *Nature*, *advance online publication*,
917 doi:10.1038/nature18273.
918 Papritz, L., S. Pfahl, H. Sodemann, and H. Wernli (2015), A Climatology of Cold Air Outbreaks and
919 Their Impact on Air–Sea Heat Fluxes in the High-Latitude South Pacific, *Journal of Climate*, *28*(1),
920 342-364, doi:10.1175/JCLI-D-14-00482.1.
921 Penny, S., G. H. Roe, and D. S. Battisti (2010), The Source of the Midwinter Suppression in Storminess
922 over the North Pacific, *Journal of Climate*, *23*(3), 634-648, doi:10.1175/2009jcli2904.1.
923 Platnick, S., M. D. King, S. A. Ackerman, W. P. Menzel, B. A. Baum, J. C. Riedi, and R. A. Frey (2003),
924 The MODIS cloud products: Algorithms and examples from Terra, *Ieee Transactions on Geoscience*
925 *and Remote Sensing*, *41*(2), 459-473, doi:10.1109/tgrs.2002.808301.
926 Qu, X., A. Hall, S. A. Klein, and P. M. Caldwell (2014), On the spread of changes in marine low cloud
927 cover in climate model simulations of the 21st century, *Climate Dynamics*, *42*(9-10), 2603-2626,
928 doi:10.1007/s00382-013-1945-z.
929 Qu, X., A. Hall, S. A. Klein, and A. M. DeAngelis (2015), Positive tropical marine low-cloud cover
930 feedback inferred from cloud-controlling factors, *Geophysical Research Letters*, *42*(18), 7767-7775,
931 doi:10.1002/2015gl065627.
932 Rayleigh, L. (1916), LIX. On convection currents in a horizontal layer of fluid, when the higher
933 temperature is on the under side, *Philosophical Magazine Series 6*, *32*(192), 529-546,
934 doi:10.1080/14786441608635602.
935 Reynolds, R. W., N. A. Rayner, T. M. Smith, D. C. Stokes, and W. Wang (2002), An Improved In Situ
936 and Satellite SST Analysis for Climate, *Journal of Climate*, *15*(13), 1609-1625, doi:10.1175/1520-
937 0442(2002)015<1609:aiisas>2.0.co;2.
938 Rosenfeld, D., Y. J. Kaufman, and I. Koren (2006), Switching cloud cover and dynamical regimes from
939 open to closed Benard cells in response to the suppression of precipitation by aerosols, *Atmospheric*
940 *Chemistry and Physics*, *6*, 2503-2511.
941 Sandu, I., and B. Stevens (2011), On the Factors Modulating the Stratocumulus to Cumulus Transitions,
942 *Journal of the Atmospheric Sciences*, *68*(9), 1865-1881, doi:10.1175/2011jas3614.1.
943 Savic-Jovcic, V., and B. Stevens (2008), The structure and mesoscale organization of precipitating
944 stratocumulus, *Journal of the Atmospheric Sciences*, *65*(5), 1587-1605, doi:10.1175/2007jas2456.1.
945 Schultz, D. M. (2001), Reexamining the Cold Conveyor Belt, *Monthly Weather Review*, *129*(9), 2205-
946 2225, doi:10.1175/1520-0493(2001)129<2205:rtccb>2.0.co;2.
947 Seethala, C., J. R. Norris, and T. A. Myers (2015), How Has Subtropical Stratocumulus and Associated
948 Meteorology Changed since the 1980s?, *Journal of Climate*, *28*(21), 8396-8410, doi:10.1175/JCLI-D-
949 15-0120.1.
950 Shao, Q. Q., and D. A. Randall (1996), Closed mesoscale cellular convection driven by cloud-top
951 radiative cooling, *Journal of the Atmospheric Sciences*, *53*(15), 2144-2165, doi:10.1175/1520-
952 0469(1996)053<2144:cmccdb>2.0.co;2.
953 Stevens, B., G. Vali, K. Comstock, R. Wood, M. C. van Zanten, P. H. Austin, C. S. Bretherton, and D. H.
954 Lenschow (2005), Pockets of open cells and drizzle in marine stratocumulus, *Bulletin of the American*
955 *Meteorological Society*, *86*(1), 51-+, doi:10.1175/bams-86-1-51.
956 Tomassini, L., P. R. Field, R. Honnert, S. Malardel, R. McTaggart-Cowan, K. Saitou, A. T. Noda, and A.
957 Seifert (2016), The "Grey Zone" cold air outbreak global model intercomparison: A cross evaluation
958 using large-eddy simulations, *J. Adv. Model. Earth Syst.*, n/a-n/a, doi:10.1002/2016MS000822.
959 Trenberth, K. E., and J. T. Fasullo (2010), Simulation of Present-Day and Twenty-First-Century Energy
960 Budgets of the Southern Oceans, *Journal of Climate*, *23*(2), 440-454, doi:10.1175/2009jcli3152.1.
961 Vogel, R., L. Nuijens, and B. Stevens (2016), The role of precipitation and spatial organization in the
962 response of trade-wind clouds to warming, *J. Adv. Model. Earth Syst.*, *8*(2), 843-862,
963 doi:10.1002/2015MS000568.

964 Webb, M., C. Senior, S. Bony, and J.-J. Morcrette (2001), Combining ERBE and ISCCP data to assess
965 clouds in the Hadley Centre, ECMWF and LMD atmospheric climate models, *Climate Dynamics*,
966 *17*(12), 905-922, doi:10.1007/s003820100157.
967 Wielicki, B. A., B. R. Barkstrom, E. F. Harrison, R. B. L. III, G. L. Smith, and J. E. Cooper (1996),
968 Clouds and the Earth's Radiant Energy System (CERES): An Earth Observing System Experiment,
969 *Bulletin of the American Meteorological Society*, *77*(5), 853-868, doi:10.1175/1520-
970 0477(1996)077<0853:catere>2.0.co;2.
971 Williams, K. D., A. Bodas-Salcedo, M. Déqué, S. Fermepin, B. Medeiros, M. Watanabe, C. Jakob, S. A.
972 Klein, C. A. Senior, and D. L. Williamson (2013), The Transpose-AMIP II Experiment and Its
973 Application to the Understanding of Southern Ocean Cloud Biases in Climate Models, *Journal of*
974 *Climate*, *26*(10), 3258-3274, doi:10.1175/jcli-d-12-00429.1.
975 Wood, R. (2006), Relationships between optical depth, liquid water path, droplet concentration, and
976 effective radius in an adiabatic layer cloud.
977 Wood, R. (2012), Stratocumulus Clouds, *Monthly Weather Review*, *140*(8), 2373-2423, doi:10.1175/mwr-
978 d-11-00121.1.
979 Wood, R., and C. S. Bretherton (2006), On the Relationship between Stratiform Low Cloud Cover and
980 Lower-Tropospheric Stability, *Journal of Climate*, *19*(24), 6425-6432, doi:10.1175/JCLI3988.1.
981 Wood, R., C. S. Bretherton, D. Leon, A. D. Clarke, P. Zuidema, G. Allen, and H. Coe (2011), An aircraft
982 case study of the spatial transition from closed to open mesoscale cellular convection over the
983 Southeast Pacific, *Atmospheric Chemistry and Physics*, *11*(5), 2341-2370, doi:10.5194/acp-11-2341-
984 2011.
985 Wood, R., and D. L. Hartmann (2006), Spatial variability of liquid water path in marine low cloud: The
986 importance of mesoscale cellular convection, *Journal of Climate*, *19*(9), 1748-1764,
987 doi:10.1175/jcli3702.1.
988 Wyant, M. C., C. S. Bretherton, H. A. Rand, and D. E. Stevens (1997), Numerical simulations and a
989 conceptual model of the stratocumulus to trade cumulus transition, *Journal of the Atmospheric*
990 *Sciences*, *54*(1), 168-192, doi:10.1175/1520-0469(1997)054<0168:nsaacm>2.0.co;2.
991 Xue, H. W., G. Feingold, and B. Stevens (2008), Aerosol effects on clouds, precipitation, and the
992 organization of shallow cumulus convection, *Journal of the Atmospheric Sciences*, *65*(2), 392-406,
993 doi:10.1175/2007jas2428.1.
994 Yamaguchi, T., and G. Feingold (2015), On the relationship between open cellular convective cloud
995 patterns and the spatial distribution of precipitation, *Atmospheric Chemistry and Physics*, *15*(3), 1237-
996 1251, doi:10.5194/acp-15-1237-2015.
997